The Meteoritical Society

Meteoritics & Planetary Science 43, Nr 1/2, 315–334 (2008)
Abstract available online at http://meteoritics.org

Carbon investigation of two Stardust particles: A TEM, NanoSIMS, and XANES study

G. MATRAJT[1*], M. ITO[2], S. WIRICK[3], S. MESSENGER[2], D. E. BROWNLEE[1], D. JOSWIAK[1], G. FLYNN[4], S. SANDFORD[5], C. SNEAD[6], and A. WESTPHAL[6]

[1]Department of Astronomy, University of Washington, Box 351580, Seattle, Washington 98195, USA
[2]Johnson Space Center, 2101 NASA Parkway, Houston, Texas 77058, USA
[3]Department of Physics and Astronomy, State University of New York at Stony Brook, Stony Brook, New York 11794–3800, USA
[4]Department of Physics, SUNY-Plattsburgh, 101 Broad Street, Plattsburgh, New York 12901, USA
[5]Astrophysics Branch, NASA-Ames Research Center, Moffet Field, California 94035, USA
[6]Space Sciences Laboratory, University of California at Berkeley, Berkeley, California 94720, USA
[*]Corresponding author. E-mail: matrajt@astro.washington.edu

(Received 14 December 2006; revision accepted 07 October 2007)

Abstract–In this work we present the results of a systematic search for cometary organics in 14 Stardust particles (particles from comet 81P/Wild 2, captured by NASA's Stardust mission) by TEM and multidisciplinary studies (XANES and NanoSIMS) of Febo and Ada, two of the organic-bearing particles identified. The combination of the three analytical techniques has established the presence of organic, cometary C in both particles. Using energy-filtered and high-resolution imaging it was shown that the C is amorphous and rare, given that it is found in grains ≤200 nm in size that are not abundant throughout the particles. The XANES maps and spectra of the carbonaceous areas identified with the TEM have shown that the carbonaceous material is organic due to the presence of carbonyl (C=O) functional groups and the overlapping of C and N on the same grains. In addition, several different C-XANES spectra were obtained from the same particle, suggesting that there is diversity in the types of carbonaceous phases present in these particles, as well as a heterogeneous distribution of the carbonaceous phases within these particles. The C-XANES spectra obtained are different from C-XANES spectra of carbonaceous chondrites and IDPs. In the particle Febo we found five spots showing a pronounced enrichment in the isotope ^{15}N ($\delta^{15}N$ from 420 to 639 ± 20 to 70‰, 1σ) that were clearly associated with the C-rich regions. The carbonaceous material has approximately solar C and D/H isotopic compositions, and the bulk O isotopic composition was found to be $\delta^{17}O = -18 \pm 13$‰ and $\delta^{18}O = -37 \pm 12$‰ (1σ). In the particle Ada we found a C-rich phase with enrichments in the isotope ^{15}N ($\delta^{15}N = 550 \pm 70$ ‰, 1σ) and the isotope D ($\delta D = 610 \pm 254$‰, 1σ). The C isotopic composition at this phase is solar ($\delta^{13}C = -4 \pm 29$‰, 1σ). The bulk O isotopic composition of Ada was found to be $\delta^{17}O = 9 \pm 14.6$‰ and $\delta^{18}O = -7.3 \pm 8.1$‰ (2σ).

INTRODUCTION

On January 15, 2006, the NASA Stardust spacecraft returned the first direct samples of cometary material, making this event the second solid sample return mission to Earth from a specific astronomical body, following only the Apollo and Luna samples returned from the Moon. Hundreds of dust particles ranging from approximately 1 μm to 100 μm in size were collected from comet Wild 2 by impact into ultra-low density aerogel with an encounter velocity of 6.1 km/s^{-1} (Brownlee et al. 2003, 2006). These particles constitute the first solid samples returned from beyond the Earth-Moon system. The samples were analyzed by an extensive Preliminary Examination Team (PET) organized into subteams that focused on studies of the organics (Sandford et al. 2006), impact features in Al foils (Hörz et al. 2006), isotopic compositions (McKeegan et al. 2006), bulk composition (Flynn et al. 2006), spectral properties (Keller et al. 2006), and mineralogy (Zolensky et al. 2006).

The identification and analysis of cometary organics in the Stardust samples are a high priority because comets preserve records of chemical processes in the early solar system and possibly in interstellar environments. Here we present the results of a systematic search for cometary organics in

Table 1. Particles surveyed with TEM.

Sample name[a]	Sample number	Sample type	General mineralogy	Carbonaceous phases
Arinna	C2,7,10	SP	FeS, forsterite	Yes
Maya	C2115,22,20	TP	Clinoenstatite	No
Aton	C2115,24,22	TP	Fe-olivine, amorphous SiO_2 (glass), Fe-sulfides, Fe-Zn sulfides	No
Inti	C2054,4,25	TP	CAI	No
Ada	C2054,5,26	TP	Crystalline SiO_2, fayalite	Yes
Sitara	C2054,5,27	TP	Enstatite, Fe sulfides	No
Tara	C2044,0,38	TP	Fe-metal, Fe-oxide, melted aerogel	Yes
Isis	C2044,0,41	Bulb	Enstatite, forsterite, melted aerogel	Yes
KeyA	C2009,1,56	TP	Enstatite, roedderite, richterite, alkali-rich glass, chromite	No
Febo	C2009,2,57	TP	Fe-Ni sulfide, enstatite, fine-grained chondritic material	Yes
Noni	C2009,3,58	TP	Fe-olivine, Al-silicate glass, Fe-oxide crystals, diopside	No
Surya	C2009,11,71	TP	Fe-rich olivine, Fe sulfides	No
Tule	C2092,3,80	Bulb	Enstatite, diopside, Ni-oxide	Yes
Puki	C2009,20,77	TP	Diopside, Fe-olivine	n.d.

[a]The official names of the particles studied during this work were supplemented by nicknames which were chosen from several antique civilizations. The meaning of most of these names is related to the words "sky, star, moon, sun..."; n.d. = not determined; TP = terminal particle; SP = side particle (fragment); Bulb = upper part of the track; CAI = Ca-Al-rich inclusion.

14 particles (Table 1) from 14 tracks (the path or cavity left in the aerogel by the impacting particle) by transmission electron microscopy (TEM) and multidisciplinary studies of 2 of the organic-bearing particles identified. Several samples (Maya, Aton, Ada, Sitara, Tara, KeyA, Febo, Noni, Surya, and Puki) were first analyzed with synchrotron radiation using X-ray fluorescence (XRF) and Fe-XANES spectroscopy (Fakra, personal communication) and Fourier transformed infrared (FTIR) spectroscopy (Bajt, personal communication) in order to have as much information as possible from the entire track before having it embedded and microtomed.

Among the 14 particles investigated by TEM, we detected the presence of C-containing areas of ~100 nm in size using energy filtered imaging (electron energy loss spectroscopy [EELS] mapping) in six of them. Two of these six particles (Febo from track 57, and Ada from track 26, Table 1) were subsequently analyzed using C-, O-, and N-X-ray absorption near-edge structure spectroscopy (C-, O-, and N-XANES) and nano-secondary ion mass spectrometry (NanoSIMS), to investigate the molecular nature and isotopic composition of the carbonaceous matter.

In this work we will first briefly describe the sample preparation and the different analytical techniques and conditions used. We will then describe the results for two particles, Febo and Ada. We will finally discuss the results by comparing the data to similar data obtained in carbonaceous chondrites and interplanetary dust particles (IDPs).

METHODS

Sample Preparation

Keystones

With the exception of two particles (Arinna and Isis), all the other particles and fragments studied were received inside aerogel keystones prepared at the University of Berkeley following the techniques of Westphal et al. (2004). Most of these keystones had been previously studied using synchrotron radiation techniques (FTIR, Fe-XANES) and were selected based on the results obtained with these techniques for further study by TEM. For example, data from XRF and Fe-XANES will determine whether or not the particle is a contaminant (piece of spacecraft) as well as its bulk mineralogy. Data from FTIR will determine whether or not there is C along the track. The keystones usually measured 1–5 mm in their longest direction and ≤0.5 mm in thickness (typically 250–300 μm). The track lengths varied from 0.2 mm to 4 mm. Most tracks have usually one particle at the end of their path which is called primary terminal particle (TP). Often some tracks also have particles that formed paths away from the main path of the track, called side tracks. The particles at the end of these side tracks are called fragments or side particle (SP). Some of the samples were primary or secondary terminal particles and some were also from track walls or track bulbs (the upper, enlarged part of the track). Table 1 provides a description of the type of particle that was analyzed from each track.

Sample Embedding and Ultramicrotomy

The keystones were processed using the "acrylic embedding" technique developed at the University of Washington (Matrajt and Brownlee 2006). Briefly, the keystone is flattened between two glass slides and a small (300 × 300 μm^2) square piece of aerogel containing the particle is cut out using a razor blade and mounted in acrylic. Ultramicrotomed sections are then prepared using a Leica ultramicrotome (Reichert Ultracut S) and a Diatome diamond knife. Since a particle with its surrounding aerogel is embedded and microtomed, each microtomed section

contains a slice of the particle and surrounding aerogel. Several sections with various thicknesses (from 40 to 95 nm) are obtained and placed over Ladd Cu or Au grids coated with ultra light amorphous C film. Prior to TEM analysis, the grids are washed using sub-boiling chloroform vapors (Matrajt and Brownlee 2006) to dissolve the acrylic and avoid interferences of the embedding medium with any possible C present in the sample. Since we did not notice any presence of Cl during the chemical analyses performed on the samples using energy dispersive X-ray spectroscopy (EDXS), we think that there were no chemical reactions with the chloroform. However, it should be noted that this procedure, besides dissolving the acrylic, would also dissolve chloroform-soluble organics from the sample if they were originally present. But chloroform is a non-polar solvent and so all the polar compounds should be preserved. Therefore, the organic materials described in the remainder of the paper represent a lower limit to the abundance and types of organics that may have been present in the original sample and are biased against chloroform soluble phases.

Analytical Techniques

Microtomed samples were investigated in the following order: First, a section was investigated with TEM to map the C throughout the sample using EELS. When carbonaceous areas were found to be ≥100 nm, the grid with the section was sent to be analyzed with XANES. A new, contiguous section was then microtomed and analyzed again with TEM to make sure that there was still C present in the sample. Then C was mapped using EELS. This new section was then sent to be analyzed with NanoSIMS to obtain C, N, H, and O isotope maps and isotope ratios. If there were any isotope anomalies present, we analyzed new sections (that were sometimes microtomed several dozens of nm down) with NanoSIMS to confirm the anomalies. Given the small size of the carbonaceous areas scanned with the NanoSIMS, a further, new contiguous section was systematically needed to measure D/H ratios, because the sections contain too little material to analyze simultaneously all four isotopes at once. We never analyzed the same section using the three techniques because the NanoSIMS technique is destructive and we wanted to preserve the sections where we found organic phases using XANES for further analysis with other analytical techniques.

Transmission Electron Microscopy

TEM images and EELS C maps of the samples were obtained at the University of Washington, using a 200 kV Tecnai F20 FEG STEM electron microscope equipped with an energy dispersive X-ray (EDX) detector and a Gatan Imaging Filter (GIF) detector.

Briefly, the sample is scanned with the electron beam and all the electrons that lose energy when traversing the sample are measured with an electron energy spectrometer (the GIF detector). This energy depends on the nature of the sample. For example, if the area traversed contains C, for which the energy edge is at 285 eV, then a peak at this energy will be detected. Using an energy filter detector, it is possible to map the element distribution through a scanned area by inserting an energy-selecting slit at the spectrum plane and at a particular energy. For the example of C, if we insert a slit at 285 eV we can form a C image, and thus map the distribution of C throughout the area scanned. To avoid artifacts and interferences from the energy coming from other elements that might be present in the area scanned, we use the three window method, which consists of obtaining two images below the C edge energy (pre-edge images) and one image above this edge (post-edge image). Then, by subtracting the pre-edge images from the post-edge image one can obtain a very accurate map with improved signal/noise.

Another modality of the GIF detector is that an image can be obtained from all those electrons that traverse the sample without losing energy. This is called the zero loss peak (ZLP) image and it is usually similar to the bright field (BF) image but with more contrast. The GIF detector was used to acquire C maps and ZLP images under the energy filtered imaging mode and the analytical conditions were as follows: slit centered at the C edge (285 eV); the three window method was used as follows: Post-edge window = 10 eV; pre-edge window #1 = 32 eV; pre-edge window # = 11 eV; slit width = 20 eV; acquisition time from 10 to 15 s; spot size 3 (20 nm); gun lens 4; and extraction voltage 4200 V.

The high-resolution images were taken using conventional TEM in bright field mode. Other images were taken in scanning transmission electron microscopy (STEM) mode using high angle annular dark field (HAADF) and secondary electrons (SE) detectors (analytical settings used: spot size 1–2 nm; camera length 200 mm). An EDX detector (EDAX) was used for chemical analysis (analytical conditions: tilt of 15°; nanoprobe spot size of 1 nm; acquisition time of 10–180 s). This detector is used to measure the X-rays emitted by electrons that have been displaced from their original electronic shell. The energy of the X-rays emitted is unique to each element and thus by measuring it one can determine the exact elemental composition of the sample analyzed.

NanoSIMS

The C, N, H and O isotopic compositions of the particles were determined with the Johnson Space Center NanoSIMS 50L ion microprobe following the TEM analyses. Images of $^{12}C^-$, $^{13}C^-$, $^{12}C^{14}N^-$, $^{12}C^{15}N^-$, $^{16}O^-$, $^{17}O^-$, and $^{18}O^-$ were acquired simultaneously in multidetection with electron multipliers. The isotopic images, covering an 8 × 8 μm^2 field of view for Febo, or a 10 × 12 μm^2 field of view for Ada were acquired by rastering a 16 keV, 1 pA Cs^+ primary ion beam

focused to 100 nm. We acquired 10 images of the sample over a period of 2 hr. Sample charging was mitigated by coating the sample with 8 nm of Pd/Au prior to the isotopic measurements and with the use of an electron flood gun during the analysis. Nearby grains of 1-hydroxybenzotriazole hydrate, biotite (NIST), USGS24 graphite, and San Carlos olivine were measured as N, H, C, and O isotopic standards, respectively. The amorphous C film substrate served as a secondary isotopic standard, providing an isotopic reference during the sample analysis. The surrounding aerogel and a sample of the acrylic used as the embedding medium were also measured and their isotopic values were found to be normal.

The uncertainties quoted for the isotopic images or regions within them that were obtained in the two particles analyzed include the counting statistical error, the measurement error of the isotopic standards (e.g., San Carlos olivine, 1-hydroxybenzotriazole, etc.), and take into account the variation of isotopic ratios among 3–5 blocks of image planes for any given region of interest. The final error is calculated from these individual uncertainties according to standard error propagation procedures.

Scanning Transmission X-ray Microscopy and XANES Microspectroscopy

The chemical bonding of the carbonaceous materials of Febo and Ada were determined with the Scanning Transmission X-ray Microscope (STXM) located at the X1A beamline at the National Synchrotron Light Source at Brookhaven National Laboratory. Febo was analyzed at the C, O, and N K shell edges and Ada was analyzed only at the C and O K shell edges. The beamline entrance and exit slits were set to 25 microns resulting in an energy resolution for the C K edge of 0.05 eV, for the N K shell edge of 0.12 eV and for the O K shell edge of 0.2 eV. For the C K shell edge, CO_2 was used to calibrate the spherical grating monochromator position, O_2 was used to calibrate the grating for the O K shell edge and N_2 was used to calibrate the grating for the N K shell edge. A Gaussian peak fitting program is used to calculate the peak position of the 292.74 eV Rydberg resonance for CO_2 and 406.1 eV resonance for N_2 with a standard deviation from the peak fit of 0.129 eV. TEM grids with the sample sections were attached to the STXM sample mounts.

The samples were analyzed at ambient pressure and temperature. For imaging, the sample was raster scanned through the area of interest. The X-ray beam at X1A is focused initially using a toroidal mirror and spherical grating monochromator. This focused beam is used to fill a 160 μm in diameter zone plate with the width of the outer most zones being 30 nm. The zone plate acts as a lens and the size of the focused beam is determined by the width of the outer most zones of the zone plate. X-rays are transmitted through the sample and for the C K shell edge a gas proportional counter was used to collect the transmitted photons. A solid state, silicon, segmented detector was used at the N K shell edge. The insertion device at the X1A beamline has both second and third order harmonics. Order sorting mirrors are used to filter out these harmonics. To eliminate higher order contamination from the zone plate an order sorting aperture is placed at the appropriate distance from the zone plate, this distance being dependent on the energy.

For spectroscopy two different methods are used at the X1A beamline. With one method called point spectroscopy, the focused beam remains stationary on the sample and the spherical grating monochromator is moved through the energy range. For the C K shell edge we used an energy range of 280–310 eV, for the N K shell edge an energy range of 390–420 eV, and for the O K shell edge we used an energy range of 520–560 eV. Because the X-ray beam is not perfectly aligned to the specimen it is difficult to keep the beam on sub-micron sized particles as one changes the energy. To eliminate this problem a method called STACKS was developed at X1A beamline (Jacobsen et al. 2000). With this method, a series of images are collected at small, incremental changes in energy. The increments in energy used for the samples in our work were as follows: for C, from 280–283.6 eV the increment was 0.3 eV; from 283.6–292.0 eV the increment was 0.1 eV; and from 292–310 eV the increment was 0.3 eV. For O, from 520–528 eV the increment was 0.3; from 528–540 eV, the increment was 0.15; and from 540–560 eV the increment was 0.6. The images can then be spatially aligned in X and Y so that it is possible to collect spectra from single pixels in the images. The spectra used in this study were collected using STACKS. Pixel sizes of 40 nm were used. From the STACKS data set the statistical tools principal component analysis (PCA) and cluster analysis were used to further analyze the data (Lerotic et al. 2004). The spectra reported in this study were all obtained from STACKS. We used PCA/Cluster analyses only to find regions where there were clusters of C or N. Also, we express all spectral data in this study in terms of optical density or D = ln(I/I0) as is common practice in X-ray absorption spectroscopy. This is related to a somewhat less common practice of expressing the data in absorbance units (AU), where AU = $log_{10}(1/10)$, the difference between these two units being a simple factor of ln(10) = 2.30, both units are linear with respect to the thickness of the sample. All the spectra discussed in this work were obtained either from the STACKS data set or the cluster data set. This methodology has been extensively used in the past for the characterization of C in meteorites and interplanetary dust particles (Flynn et al. 2003, 2004; Keller et al. 2004) as well as in Antarctic micrometeorites (Matrajt et al. 2001).

In this work we mapped two samples, Febo and Ada. We used C, O and N-XANES to localize the C, O, and N throughout the microtomed section. We then acquired the C and O-XANES spectra at different areas of the sample looking at single pixel spectra as described above. No N-XANES

spectra were obtained because the N concentration in the samples was too low to obtain good signal/noise (S/N) and accurate spectra. The different spectra obtained are the ones discussed in the following sections and shown in the figures.

Sample Selection

Table 1 lists the sample names and numeric identifications of the Stardust particles that were analyzed with TEM and provides a brief description of their main mineralogy. A detailed description of the mineralogy of these particles will be available in the online Stardust catalog (Joswiak, Zolensky, personal communication).

Out of the 14 particles surveyed during this study, only one of them, Febo, has fine-grained material (Brownlee et al. 2006). All the other particles are solid rocks composed of a single mineral or the combination of two or three minerals. Therefore, C was not expected to be found in most of the particles because of the lack of fine-grained material. Despite the lack of fine-grained particles, carbonaceous phases were detected in six of the particles listed in Table 1. Most of these carbonaceous phases are smaller than 100 nm in size. For the present study, we looked for samples where the carbonaceous areas would be ≥100 nm in size because this is the minimum size required for accurate isotopic measurements. Two of the particles having carbonaceous phases at least 100 nm in size (see Figs. 1 and 2) were selected for isotopic measurements by NanoSIMS: Febo (after the Roman god of the Sun) and Ada (after the Assyrian god of the Sun) and the discussion below will concentrate only on the description of those two particles.

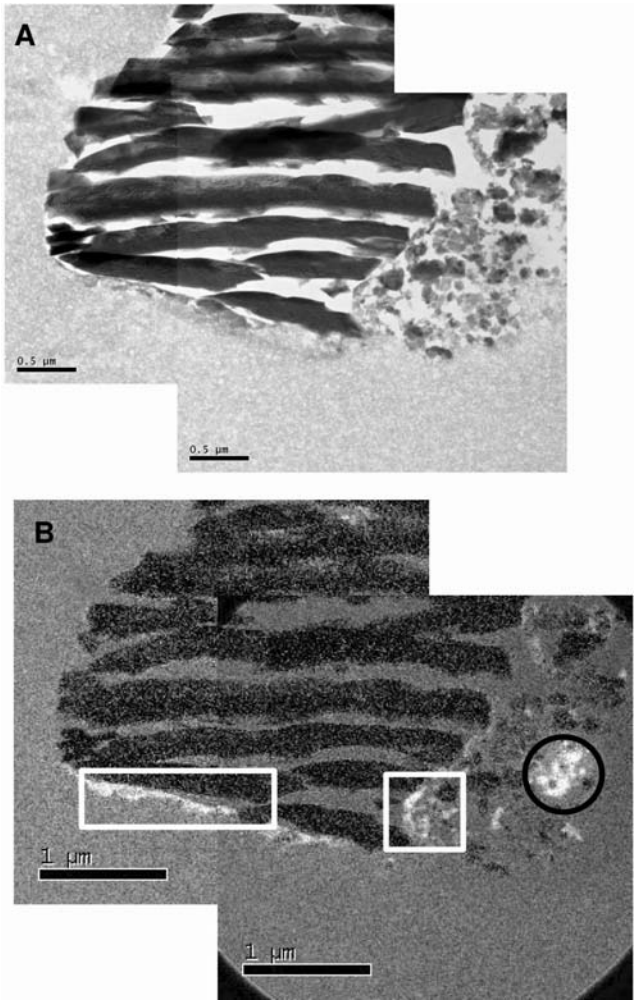

Fig. 1. TEM images of the area in Febo where C was found. a) Zero-loss image obtained with the zero loss peak (ZLP) of the area of the particle where C was most abundant. b) C-EELS map: the bright regions in this micrograph are the C-rich areas, and the dark region with elongated and sharp features is the sulfide. Three main C-rich areas (white) can be distinguished (noted by a rectangle, a square, and a circle).

RESULTS FOR FEBO

TEM Analysis

Brief Description of the Mineralogy of Febo

Febo is an 8 µm terminal particle composed of three main regions (Fig. 3): one region is made of a large Fe-bearing sulfide with trace Ni, which is believed to be pyrrhotite; the second region is a piece of enstatite and the third region is the surrounding fine-grained material which has chondritic chemical composition (Mg, Al, S, Ca, Fe, Ni ratios = solar) except for Si because of its significant contribution from aerogel (Brownlee et al. 2006).

Carbon Maps with Energy Filtered Imaging

The distribution of C within Febo was mapped by energy filtering with a 10 s acquisition time. The zero loss image (which is equivalent to the bright-field image but with slightly more contrast) and the C map are shown in Fig. 1. The bright areas in the C map represent locations that are C-rich. Three main areas can be distinguished (noted by the rectangle, square, and circle in Fig. 1) and shown in Figs. 4 and 5; these are discussed in the next sections.

High-Resolution Imaging of the Carbonaceous Areas

Figure 4 shows high-resolution (HR) images of the carbonaceous areas of the particle Febo, that are found inside the areas denoted by the rectangle and square in Fig. 1. Figures 4b and 4d show amorphous C with some order compared to the C support film next to it. This order is evident from the subparallel fringes that form on C that has been slightly heated, as opposed to the parallel, 3.4 Å spaced fringes, which are associated to very well ordered C such as graphite, or the structureless C of the amorphous C film that has not been heated. When C is heated, there are structural changes that can be observed with HRTEM. Growth and

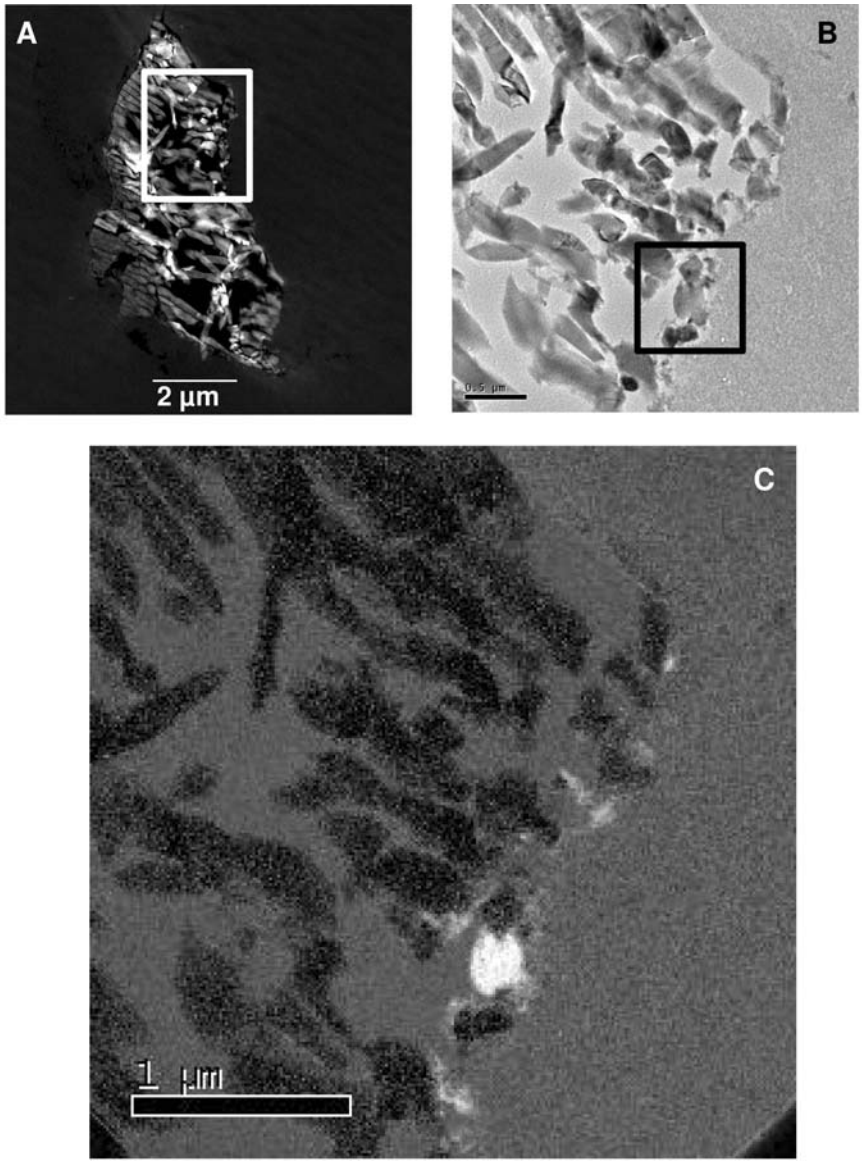

Fig. 2. TEM micrographs of Ada. a) Micrograph taken with STEM mode (HAADF detector) of the whole particle. The square indicates the location in the particle where the carbonaceous area is found and it is shown magnified in (b). b) Micrograph taken with TEM conventional mode (bright field). The area with carbon is denoted by a black square. c) Carbon map taken with energy filter imaging mode (EELS detector). The white areas are those that contain carbon.

stacking of planes with C atoms become visible, from subparallel fringes, passing through layers arranged concentrically to layers stacked regularly at spacings of 3.4 Å (Buseck and Bo-Jun 1985). The HR images of C-rich areas in Febo show subparallel fringes typical of a poorly ordered C that has been slightly heated (Buseck and Bo-Jun 1985). The comparison of these fringes to those reported in HR images of annealed carbonaceous compounds (Buseck et al. 1987; Matrajt et al. 2005) show that the fringes observed in Febo are similar to the structures of compounds that were annealed at temperatures around 1000 °C, suggesting that these two particles were heated at around 1000 °C or less during entry and deceleration in the aerogel. Alternatively, this slightly heated state of the C observed in these samples is indigenous and the heating event occurred in the parent body.

Figure 5a shows a higher magnification of the carbonaceous area seen inside the circle in Fig. 1, obtained with energy-filtered imaging mode. Figures 5b and 5c show two images obtained in STEM mode of the same region. This area looks like a doughnut and will be referred to by this name here. The EDX spectrum of the spot analyzed at the center of the doughnut is also shown in Fig. 5d. This EDX spectrum shows an Fe-sulfide with some contribution from the surrounding C. The presence of sulfides intermixed with the carbonaceous phases suggests that the C was originally present in the particle, prior to its capture in aerogel.

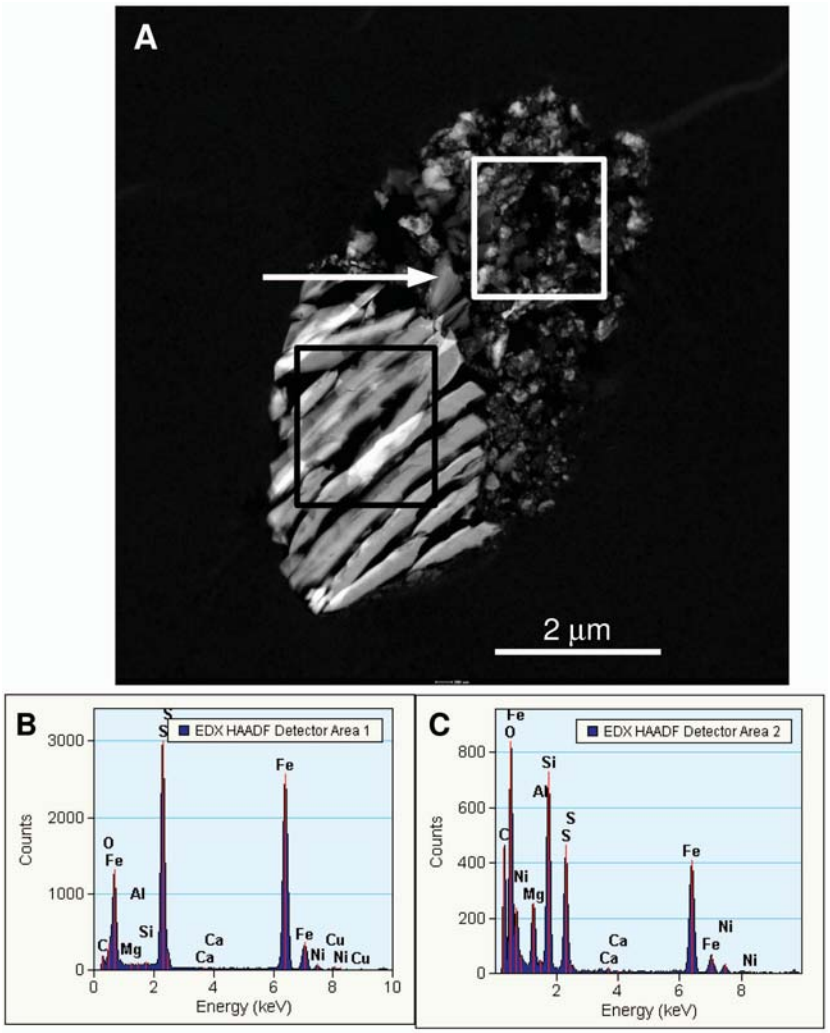

Fig. 3. STEM data of Febo. a) HAADF micrograph. The black box shows the rastered area (area 1) over the sulfide that corresponds to the EDX spectrum shown in (b). The white box shows the rastered area (area 2) over the fine-grained material that corresponds to the EDX spectrum shown in (c). The white arrow points to the enstatite grain. The analytical EDX conditions were: 180 s, nanoprobe spot size 5 (2–3 nm), tilt 15°, camera length 200 mm.

Isotopic Measurements

The carbonaceous material in Febo identified by TEM was also identified in CN^- isotopic images obtained by NanoSIMS (Fig. 6a). However, the C-rich regions are not distinguished in C images due to the significant signal originating from the amorphous C substrate. The NanoSIMS analysis also suffered from a significant background of N, whose origin is unknown. This background was also observed with XANES (see next section). Neither the acrylic nor the chloroform contain N in their structure, therefore one possible explanation for the observed N background is that atmospheric N may have been absorbed in the aerogel, which is an extremely porous material. But this possibility, which remains a hypothesis, has not been further explored. A strong N background has also been observed in other NanoSIMS analyses of particles embedded in epoxy (Messenger et al. 2007) which did not preclude the obtention of good quality measurements. Despite these limitations, a pronounced enrichment in ^{15}N ($\delta^{15}N = 420 \pm 160‰$, 1σ) is clearly identified with the C-rich region in Febo containing the doughnut shaped material described above. In addition, in another thicker (80 nm) microtomed section of Febo where more isotopic analyses were performed, five separate CN^--rich spots were identified (Fig. 7a). Four of these spots showed pronounced enrichments in ^{15}N: spot N1 has a $\delta^{15}N = 639 \pm 28‰$; spot N2 has a $\delta^{15}N = 518 \pm 71‰$; spot N3 has a $\delta^{15}N = 479 \pm 21‰$; and spot N4 has a $\delta^{15}N = 591 \pm 28‰$; (errors are 1σ). Only spot N5 ($\delta^{15}N = -20 \pm 32‰$) has normal N isotopic composition within error. The carbonaceous material at all these spots has approximately solar C isotopic composition within broad error limits arising from the small size of the sample.

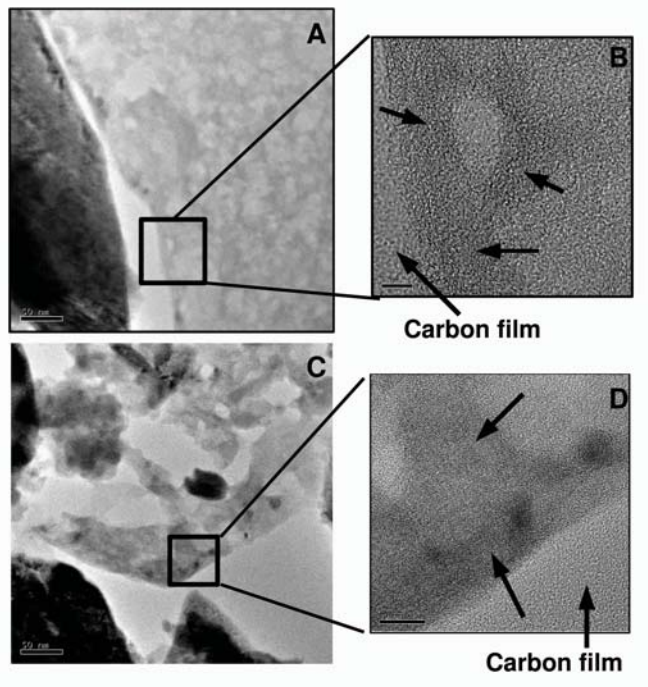

Fig. 4. High-resolution images in TEM mode of two of the carbonaceous areas in Febo (shown in white in Fig. 1). a) From rectangle in Fig. 1 and (c) from square in Fig. 1. The scale bar is 50 nm. (b) and (d) are, respectively, a blow-up of the areas denoted by a square in (a) and (c). The scale bar in (b) is 5 nm. The scale bar in (d) is 10 nm. Both (b) and (d) images show an amorphous C (pointed by thin arrows) with little structure (subparallel fringes) compared to the C film next to it.

The bulk O isotopic composition of the sample was found to be $\delta^{17}O = -18 \pm 13‰$ and $\delta^{18}O = -37 \pm 12‰$ (1σ) relative to the standard mean ocean water (SMOW). For the enstatite grain in Febo, we measured a $\delta^{17}O = -39 \pm 22‰$ and $\delta^{18}O = -18 \pm 4‰$ (1σ).

Another section of Febo was measured for its H isotopic composition by isotopic imaging. Although a strong background of H and C was observed from the aerogel surrounding the particle, this was removed by prolonged sputtering. Several submicrometer C and H rich regions were observed, and their D/H ratios were determined to be within approximately 300‰ of the terrestrial SMOW standard.

Carbon, Nitrogen and Oxygen X-Ray Imaging and XANES Analysis

A microtomed section (contiguous and ~50 nm away in thickness from the section analyzed with NanoSIMS) of the particle Febo was imaged below the C K-shell edge (280–283 eV) and above the edge (292–296 eV) to map the C distribution; the particle was also imaged below the N K-shell edge (390–395 eV) and above the edge (415–420 eV) to map the N distribution; and below the O K-shell edge (520–528 eV) and above the edge (540–560 eV) to map the O distribution throughout the particle. Then C and O XANES spectra were collected from the areas enriched with these elements.

Carbon

Figure 8a shows the distribution of C of this new microtomed section obtained from the ratio of the averaged pre-edge images to the average of the above edge images. Figure 8b shows its EELS C map. Since this is a several nm deep new microtomed slice, as it was described in the Analytical Techniques section, the C-EELS map is similar, but not identical, to the C-EELS map shown in Fig. 1b. We pointed the different C-rich areas in the C-EELS map of Fig. 8b with boxes and from the comparison of their locations relative to the C-rich areas shown in Fig. 1b, we think that the doughnut corresponds to the C-rich spot located inside box 4 in Fig. 8b. Figure 8c shows a plot with C-XANES spectra corresponding to the several C-rich areas shown inside the boxes in Fig. 8b.

The bright areas (areas with highest optical density) of the C absorption map in Fig. 8a nicely overlap the C-rich areas of the EELS C map (Fig. 8b) showing that the C distribution is real at all spots and not the product of any analytical artifact.

The C-XANES spectra shown in Fig. 8d vary with the areas analyzed. For example, spectrum #1 is different from all the other spectra. This shows a diversity in the types of carbonaceous phases present, as well as a heterogeneous distribution of these different materials. Spectrum #1 shows a narrower 285 eV peak (which corresponds to a C=C bonding) than the corresponding peaks in the spectra below. In addition, spectrum #1 shows a peak at 288.5 eV (which can be assigned to a C=O bond) which is absent in the spectra below. This suggests that at least one area of Febo may have an organic carbonaceous compound containing a carbonyl functional group. There are multiple reasons for the presence of a broad 285 eV peak. For example, there could be several different bonds and these peaks would overlap to form one large peak. Alternatively, large aromatic compounds have peaks on either side of a 285 eV peak due to the symmetry of the ring structure. If this structure is disordered this results in one broad peak. This suggests that there is not a single carbonaceous compound responsible for the 285 eV feature but rather this peak is the result of the presence of several different compounds.

Figure 9 shows a comparison of C-XANES spectra of one Febo location (spectrum #1) with a C-rich area located in particle Ada (see next section) and with C-XANES spectra of other extraterrestrial samples, i.e., Murchison, Tagish Lake, IDPs (from Flynn et al. 2003, 2004 and Keller et al. 2004) that were obtained with the same instrument and under the same analytical conditions. It is important to note here that for the indigenous C-containing compounds in the meteorites listed and for the IDPs the spectra used in this plot are picked from several different C-XANES spectra from each meteorite or

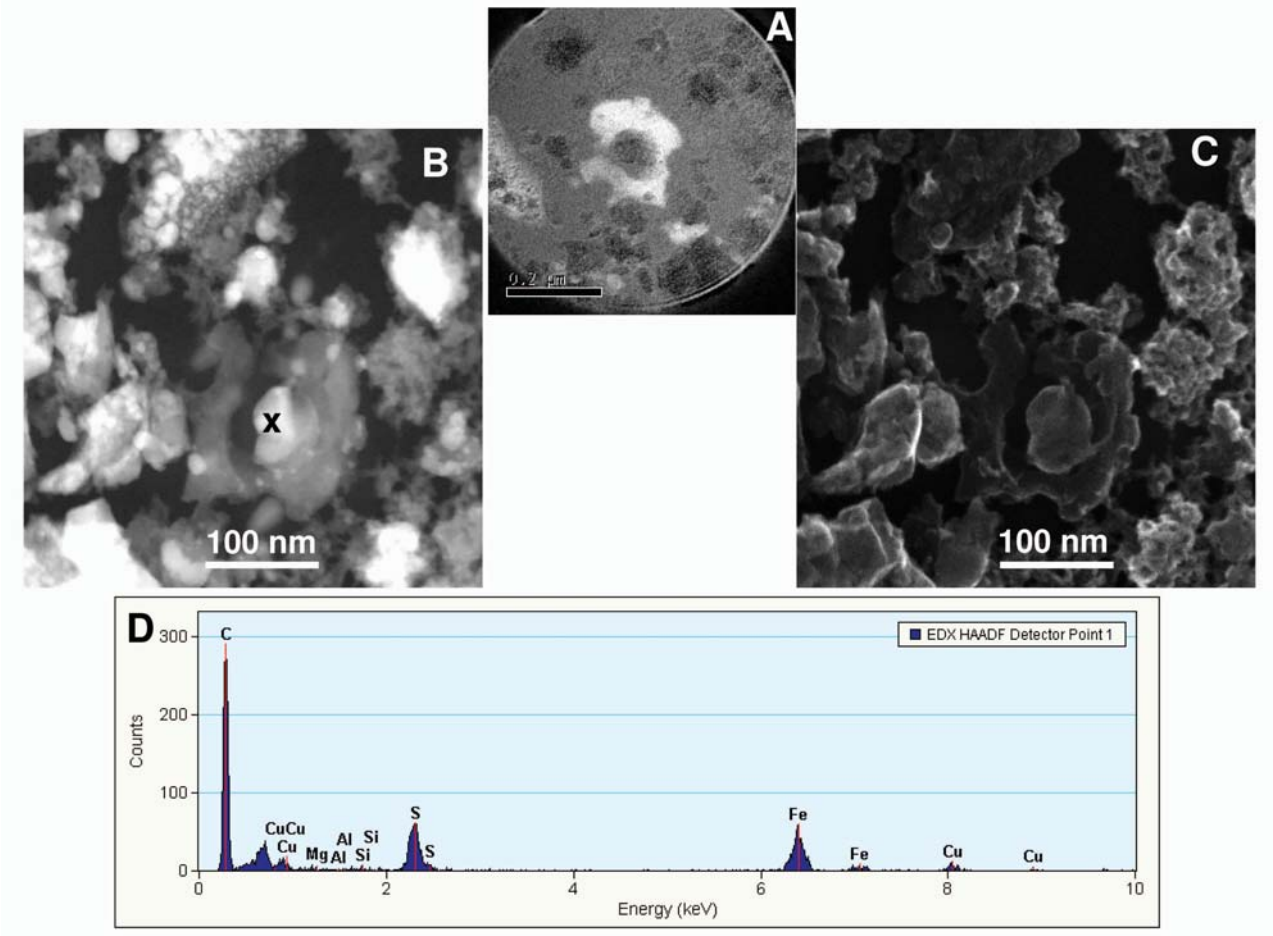

Fig. 5. TEM images of Febo. a) Magnified C-map image of the doughnut area, that was shown inside a circle in Fig. 1). b) HAADF image of the doughnut; the X indicates the EDX analytical spot. c) SE image of the doughnut. d) EDX spectrum corresponding to the analytical spot X, indicated in (b). The spectrum shows a Fe-sulfide composition with some contribution of the surrounding carbon.

IDP. The spectrum of Febo shown in this plot was chosen because it is slightly similar to the spectrum of Murchison (indigenous). This similarity is observed in the overall aspect of the spectra: the position, shape, and height of both peaks at 285 eV and 288.5 eV. However, in the Murchison (indigenous) spectrum there is a feature at 292 eV that is absent in the Febo spectrum and the 285 eV peak of Febo is broader than the 285 eV peak of Murchison. The spectra of other areas of the Febo thin section (Fig. 8c) do not show any similarity with the spectra of meteorites and IDPs, and so they were not compared in Fig. 9.

Nitrogen

The X-ray absorption maps of Febo confirm, as did the NanoSIMS, the presence of N-containing compounds in Febo. Although we could confirm the presence of N on the sample, data on N is not available because there is not very much of it present in the sample (for STXM, a 1–2% concentration of N is required to obtain correct spectra). The spectra we obtained (not shown) have features that are too broad to make any guesses as to the N chemistry. In addition, as it was observed with NanoSIMS, there is a N background in this section which also interferes for the interpretation.

Oxygen

Figure 10 shows O-XANES spectra and an absorption map obtained from Febo. The bright areas of the O absorption map overlap some of the bright areas observed in the C absorption map (Fig. 8a) showing that the C in some of these areas is linked to O. Some areas in the O absorption map do not overlap with the C absorption areas, suggesting that the O at these localities is linked to a mineral phase or to aerogel. Some other areas show an overlapping of both O and C. However, their C-XANES spectra do not show the presence of a carbonyl (C=O) feature at 288.5 eV, suggesting that the O at that particular spot is not linked to a carbonaceous phase but rather to a contiguous mineral or to a piece of aerogel. For example, spectrum #1 (Fig. 8c) shows a 288.5 eV peak and the area 1 in both the C map (Figs. 8a and 8b) and the O map

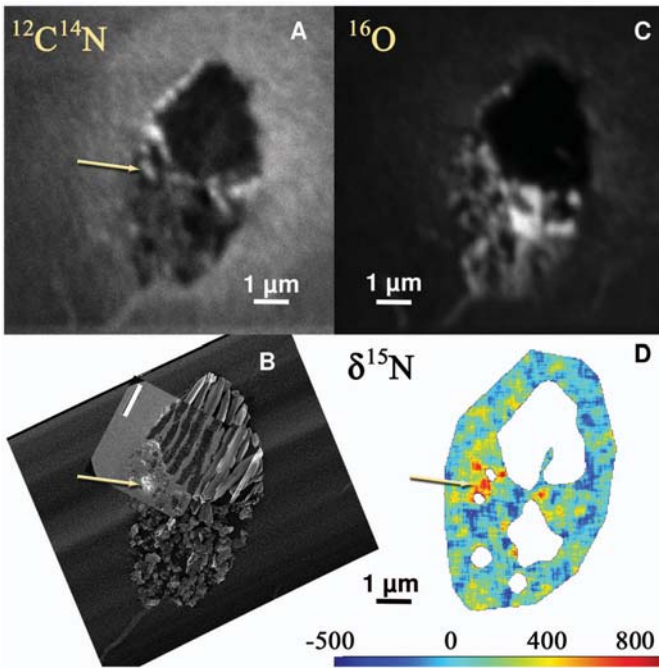

Fig. 6. Isotope maps of Febo. The arrow indicates the position of the C-rich doughnut discussed in the text and denoted by a circle in Fig. 1. a) CN^- image of Febo. b) EELS C map overlain on a SE image of Febo. c) ^{16}O image of Febo. The brightest area corresponds to a ~0.5 µm enstatite grain and the surrounding O-rich material is fine grained chondritic material. d) False color $\delta^{15}N$ image of Febo, with low-signal surrounding background masked. The hot spot shown by an arrow has a $\delta^{15}N$ value of 420 ± 160‰ (1σ).

(Fig. 10a) shows that C and O overlap. By contrast, areas #2 and #6 of the C and O map of Febo, which also have C and O overlapping, do not show the presence of a peak at 288.5 eV in the corresponding C-XANES spectra (Fig. 8c), suggesting that the O in these areas is linked to a mineral phase that may be very close (or maybe underneath) to the carbonaceous phase. It is therefore required to have both O and C maps and spectra at a single spot to accurately determine the presence/absence of a carbonyl (or any other O-bearing carbonaceous bond). The lack of the 288.5 eV feature will strongly suggest that the O is indeed linked to the minerals (or aerogel) surrounding the carbonaceous area.

RESULTS FOR ADA

TEM Analysis

Ada is a 12 µm terminal particle composed of multiple nodules of fayalite each surrounded by rims of crystalline SiO_2 (which is believed to be tridymite, Fig. 2). Ada was mapped using the same energy filtered imaging analytical conditions as used for Febo. The bright field image and C map for Ada are shown in Figs. 2b and 2c, respectively. Only one bright area in the C map was observed, showing that C in this particle is even more rare than in Febo. This C-rich area

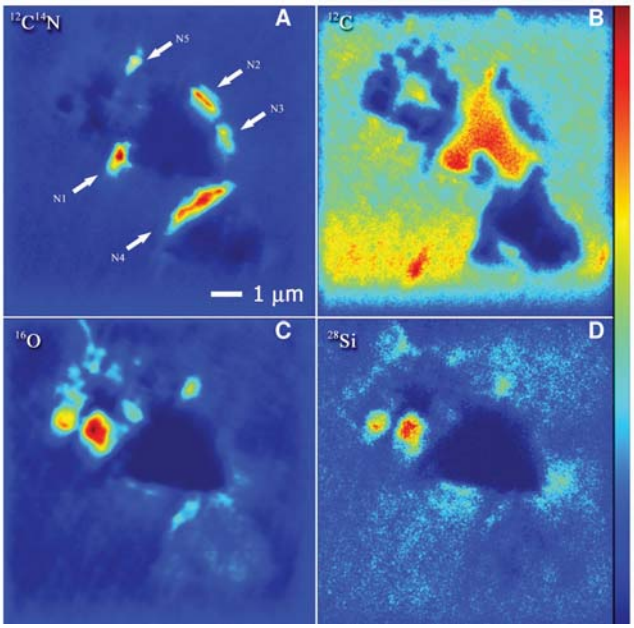

Fig. 7. False-color isotope images of a new (several dozens of nm down) section of Febo. The images in this figure have been convolved with 3 × 3 pixel kernel, so that the counts at each pixel correspond to the sum over nine adjacent pixels covering a 60 × 60 nm area. The images are all displayed using the same linear color scale (shown at the right hand side of the figure), and each image is scaled to the minimum and maximum number of counts recorded in a 3 × 3 pixel bin. The ranges of counts for these images are: ^{12}C: 6-3,310; $^{12}C\ ^{14}N$: 31-2,725; ^{16}O: 131-25,500; ^{28}Si: 1-693. Given that this new microtomed slice is deeper than the one shown in Fig. 6, the overall outline looks slightly different. a) CN^- isotopic image. The arrows indicate the position of the N-rich spots discussed in the text. b) ^{12}C isotopic map. The brightest area corresponds to a hole in the section, probably a piece of the particle that plucked out during the microtomy process. c) ^{16}O isotopic image. The brightest areas probably correspond to silicate grains. d) ^{28}Si isotopic image. The brightest area, that overlaps the brightest area in the ^{16}O isotopic map, probably corresponds to silicate grains. The location of the carbonaceous target in the section identified by TEM is identified in the NanoSIMS CN^- map by aligning the ^{16}O and ^{28}Si isotopic maps of the minerals surrounding the C-rich target.

is in the most external part of the particle (at the edge) and, unlike Febo, is not surrounded by fine-grained material but rather by SiO_2 and fayalite. No HR images of the C in Ada are available.

Isotopic Measurements

The carbonaceous material in Ada identified by TEM was also identified in D isotopic images (Figs. 11a and 11b) and CN^- isotopic images (Figs. 11c and 11d) obtained by NanoSIMS. A pronounced enrichment in ^{15}N ($\delta^{15}N = 550 \pm 70$‰, 1σ) is clearly identified with the C-rich region in Ada (Fig. 11d). The ^{15}N enrichment found in the carbonaceous material of Ada is clearly distinct from the values measured in the background of the sample (film, aerogel): $\delta^{15}N_{bulk} = 10 \pm 5$‰, 1σ.

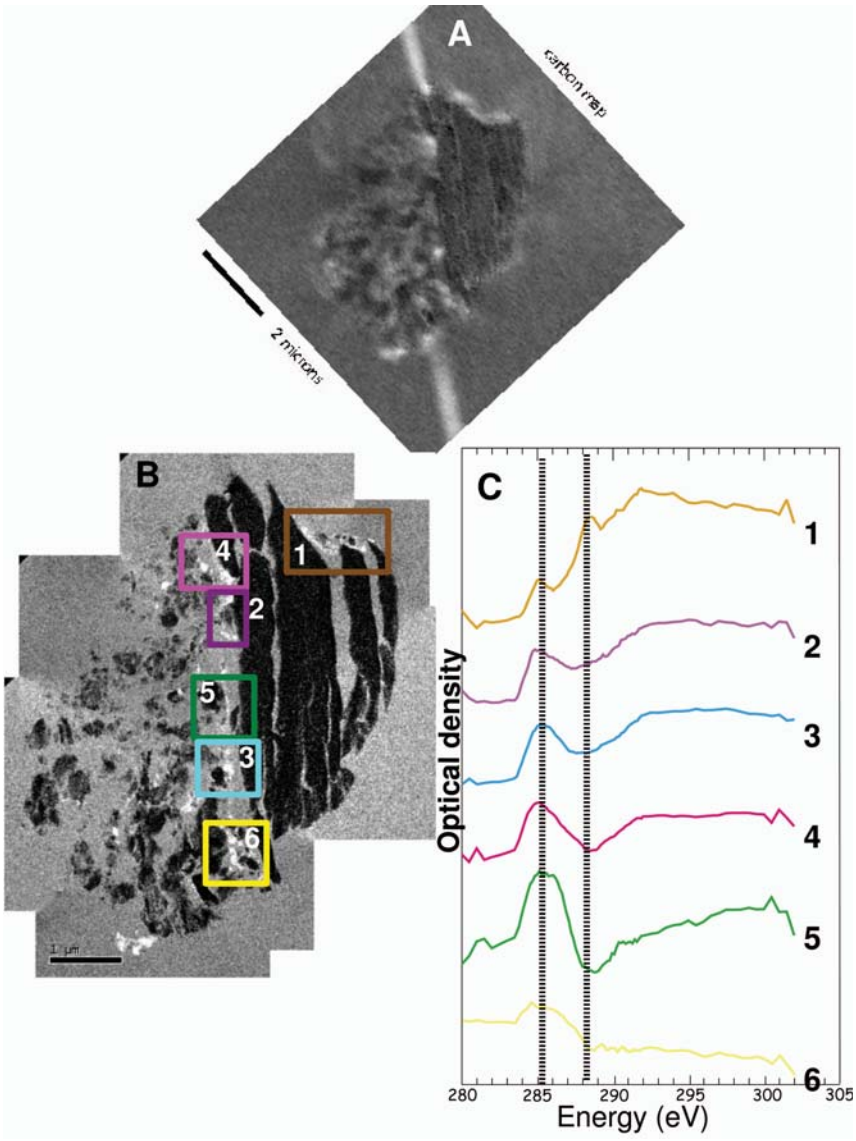

Fig. 8. C-XANES map and spectra of Febo. This is a contiguous section, several nm deeper than the section shown in Figs. 1 and 3. The difference in depth makes the overall outline of this new section slightly different. a) C-XANES map. The brighter areas are C-rich. The white, diagonal line is an artifact from the film (substrate) of the grid. For comparison, the EELS C map of this section is shown in (b). C) C-XANES spectra of different C-rich areas, shown inside the boxes of the map in (b). Boxes 1, 2, and 4 show C-rich areas that are in a similar location as the C-rich areas shown in the C-EELS map of Fig. 1. We think that the doughnut corresponds to the location of box # 4.

An additional thicker (80 nm) microtomed section of Ada, a few nm away from the section used for N isotopic measurements, was measured for its H isotopic composition by acquiring images of H, D, ^{12}C, ^{16}O, and ^{18}O simultaneously over a 10 micrometer field of view (Fig. 11a). These images were acquired with a moderately stronger Cs^+ primary ion beam (~10 pA versus 1 pA for N images) to mitigate the H background originating from OH and H_2O in the vacuum system. The increased beam current limited the spatial resolution to approximately 150 nm, and the sample was consumed after acquiring 6 image planes. The H images were essentially uniform and dominated by background, whose average isotopic composition was found $\delta D = -180 \pm 60‰$ (1σ). Because of the low D count rate, the D/H ratio image displays widely ranging values (−800 to +1000‰) at the 200 nm spatial scale. However, only two small (200–300 nm) regions were found to have statistically significant enrichments in D ($\delta D = 610 \pm 254‰$). Since no TEM data are available for this section (because it was mounted directly over the grid bar), we used the ^{16}O image to orient and align the H isotopic images relative to the previous TEM images of the section used for N isotopic measurements. The location of the D-rich spots were found to coincide with the carbonaceous target material (Fig. 11b). In addition to the D-rich spot that coincides with the ^{15}N-rich spot, we also found another spot farther away in the section (Fig. 11b), that

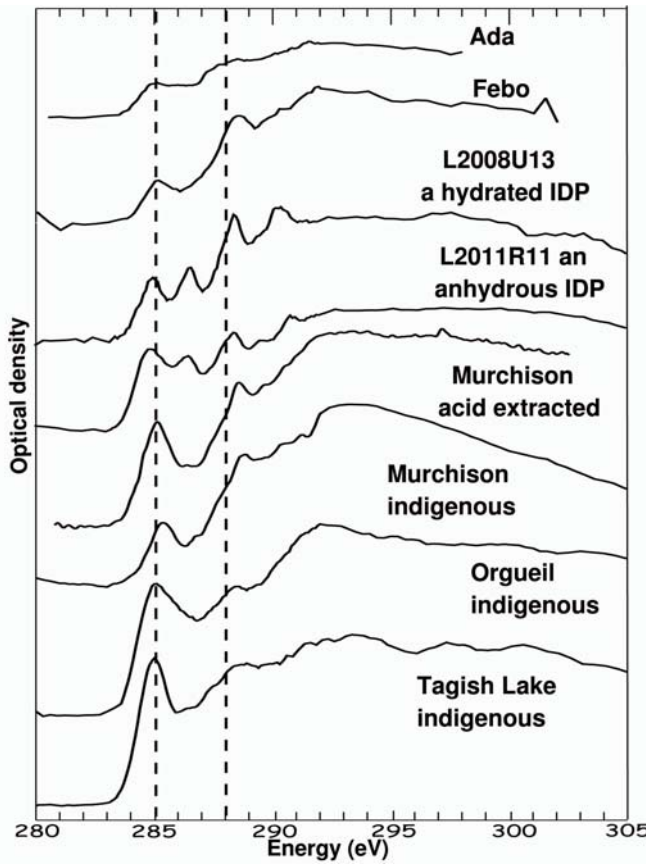

Fig. 9. C-XANES plot showing spectra of Febo and Ada compared to C-XANES spectra of the carbonaceous chondrites Murchison, Tagish Lake, Orgueil and two IDPs. All the spectra were obtained with the same instrument, under the same analytical conditions and using the same data reduction procedures, but not during the same experiment. IDPs and meteorites have typically several different kinds of C-XANES spectra. The spectra of IDPs and meteorites shown in this plot were chosen because of their closeness and similarity to the Stardust particle spectra. The spectra of IDPs and meteorites are from Flynn et al. (2004) and Keller et al. (2004). The spectra of Tagish Lake is from S. Wirick (personal communication).

we speculate to be carbonaceous material that moved when the section was laid down, during microtomy.

Carbon isotope measurements show that C at the ^{15}N-rich spot is normal ($\delta^{13}C = -4 \pm 29‰$, 1$\sigma$), i.e., indistinguishable from terrestrial or meteoritic values, or the background (film, aerogel) of the sample ($\delta^{13}C_{bulk} = -23 \pm 3‰$, 1$\sigma$).

The bulk O isotopic composition of the sample was found to be $\delta^{17}O = 9 \pm 14.6‰$ and $\delta^{18}C = -7.3 \pm 8.1‰$ (2σ) relative to the Standard Mean Ocean Water (SMOW). Two kinds of mineral grains were found near the C-rich area of Ada: crystalline SiO_2 and fayalite. The O isotopic compositions of several of these grains were measured. Oxygen isotopes in both types of crystals show homogeneous distributions and were determined to be as follows: for fayalite $\delta^{17}O = -3.1 \pm 13.9‰$ and $\delta^{18}O = -3.1 \pm 6.7‰$ (1σ); for SiO_2 $\delta^{17}O = 9 \pm 12.1‰$ and $\delta^{18}O = -10.4 \pm 5.6‰$ (1σ).

Carbon, Nitrogen and Oxygen X-ray Imaging and XANES Analysis

Similarly to Febo, a microtomed section (contiguous and ~50 nm away in thickness from the section analyzed with NanoSIMS) of the particle Ada was imaged below the C K-shell edge (280–283 eV) and above the edge (292–296 eV) to map the C distribution and below the O K-shell edge (520–528 eV) and above the edge (540–560 eV) to map the O distribution throughout the particle. Then C and O XANES spectra were collected from the areas enriched with these elements. N-XANES was not measured at this particle.

Carbon

Figure 12 shows the distribution of C throughout the microtomed section and a plot with the C-XANES spectra of the only C-rich area found in this particle. The C-XANES spectra of Ada does not show any similarity with the spectra of other extraterrestrial (ET) particles, including Febo (Fig. 9).

Oxygen

Oxygen was measured in the exact same section where C was measured (spectra and images shown in Fig. 12). Figure 13 shows an HAADF image of the area where carbon was found (Fig. 13a), an O-XANES map (Fig. 13b) and two plots with O-XANES spectra (Figs. 13c and 13d). The comparison of both C and O-XANES maps show that C overlaps with O. Therefore, the peak at 288.5 eV shown in the C-XANES plot of Fig. 12 corresponds to a C=O bond (carbonyl), showing that the carbonaceous phase at this location is likely to be organic. The O-XANES spectrum of this organic phase is slightly different from the O-XANES spectrum of an inorganic phase (silicate and/or aerogel) because the peak of the latter is centered at 537.8 eV whereas the peak of the organic phase is centered at 537 eV (Fig. 13).

Lines of Evidence Showing the Effectiveness of the Acrylic Removal with Chloroform

There are several lines of evidence showing that the acrylic is effectively removed from the ultramicrotomed sections when washed with chloroform, and that if there is any acrylic left, this residue does not interfere with the measurements of C in the cometary particles.

The XANES spectroscopy data gives one of these lines of evidence. Given that the absorption of aerogel is uniform in the 280–310 eV range, we compared the transmitted flux in the pre-edge region (281.5 eV) with the transmitted flux at 296 eV and found a 5% absorption in the aerogel area surrounding Febo and a 20% absorption in the aerogel area surrounding Ada. This absorption could be from either left-over acrylic, or the known organic material in the aerogel (Sandford et al. 2006), or differential thickness of the ultramicrotomed sections or the C substrate on the TEM grid

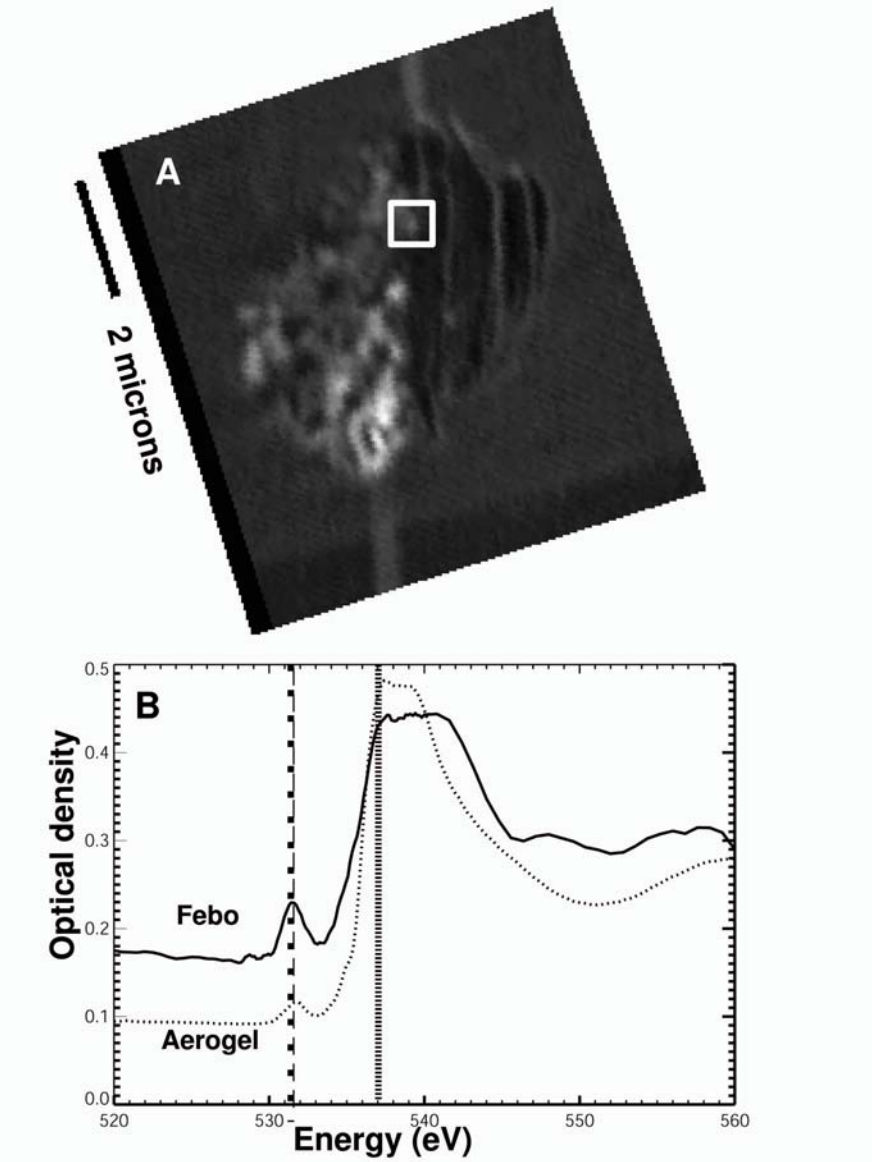

Fig. 10. O-XANES map and spectra of the same area of Febo shown in Fig. 8. a) O-XANES map. The brighter areas are O-rich. The white, diagonal line is an artifact from the film (substrate) of the grid that is folded. b) O-XANES spectrum of an O-rich area, shown inside the box of the map in (a) and for comparison, the O-XANES spectrum of bulk aerogel (courtesy of A. Butterworth).

(the transmitted flux was normalized to I_0 from a hole in the grid). The background absorption is quite different between Febo and Ada but it is important to note here that we do not know how uniformly distributed the organic contaminant is in the aerogel. If residual acrylic is the reason for this background absorption then it is likely that this error is not uniform in the sample area but will be dependent on the ability of each individual particle in the sample to absorb the embedding acrylic. However, this background C absorption from aerogel and acrylic appears to be very minimal, as it is observed in Fig. 14, showing a comparison between the spectra of aerogel surrounding particles Ada and Febo, a spectrum of the acrylic used as the embedding medium and a piece of bulk aerogel (courtesy of A. Butterworth). In this comparison, several differences in the C-XANES spectra are observed. For example, the spectrum of acrylic is dominated by a very sharp and high peak at 288.5 eV and a very small, broad peak at 285 eV whereas the spectrum of aerogel has only two small, broad peaks at 285 eV and 288.5 eV. The spectra of the aerogel surrounding Ada and Febo show an absence of peaks from the acrylic proving that the acrylic is effectively removed with chloroform from the microtomed sections. If now we compare the Febo and Ada C-XANES spectra (Figs. 8 and 12) to the spectra of acrylic and aerogel that we described above, one can notice that the spectra of Febo and Ada are significantly different from the C spectra of

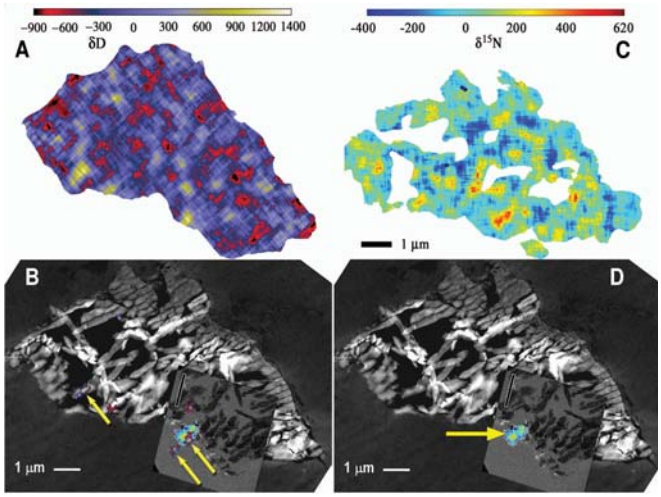

Fig. 11. H and N isotopic images of Ada. Virtually all of the apparent isotopic variations can be ascribed to statistical variations due to the very low D and ^{15}N count rates. Therefore, only areas showing statistically significant (≥2σ) H and N isotopic anomalies are overlain on the TEM images below. a) δD isotopic image of Ada. The δD image has been aligned and scaled with a secondary electron TEM image b) by using the simultaneously acquired ^{18}O image that originates from the silicate material in Ada. The outline of the ^{18}O image has been used to define the exterior of the δD image. b) Statistically significant (≥2σ) D-rich areas (purple spots) overlain on the secondary electron TEM and EELS C map images of Ada. Two of the arrows indicate the position of the D-rich spots (δD = 610 ± 254‰, 1σ) discussed in the text and correspond to the position of the carbonaceous material identified by EELS. A third arrow indicating another D-rich spot (farther left) may be due to carbonaceous material that moved from the periphery of the particle when the section was laid down, during microtomy. Note that the SE micrograph used in this image was obtained from a section ~100 nm away from the section measured for D/H. (C) ^{15}N isotopic image of Ada. The ^{15}N image has been aligned and scaled with the secondary electron TEM image (d) with the simultaneously acquired ^{16}O image that originates from the silicate material in Ada. The outline of the ^{16}O image has been used to define the exterior of the ^{15}N image. d) Statistically significant (≥2σ) ^{15}N-rich areas of Ada (blue spot) overlain on a secondary electron TEM and EELS C map images of Ada. The ^{15}N hotspot ($\delta^{15}N$ value of 550 ± 70‰, 1σ) is indicated with the yellow arrow.

acrylic or background C contamination in the aerogel. For example, the C spectrum of Ada (Fig. 12) shows a higher and broader peak at 285 eV than in the aerogel and a very small and broad peak at 288.5 eV. The dominant, sharp peak at 288.5 eV of acrylic is absent in the C spectrum of Ada. On the other hand, the C spectra of Febo (Fig. 8) have either a higher and broader peak at 285 eV than the aerogel and no peak at 288.5 eV (spectra #2–6) or a higher and less broad peak at 285 eV than the aerogel and a smaller and less sharp peak at 288.5 eV than the acrylic (spectrum #1).

A second line of evidence comes from the data obtained with TEM imaging. When acrylic is present in the sections (when it has not been removed with chloroform) it usually appears as a lacy vesicular material filling up spaces between mineral grains (images not shown). This lacy vesicular material is absent in those sections that have been washed with chloroform (e.g., Fig. 2). In addition, the peak of C in the EDX spectra tends to be higher than 500 counts when acrylic is present in the section, but it is usually very small in sections where acrylic has been removed (see Fig. 3b), unless the area analyzed contains C (see Fig. 3c).

Finally, a third line of evidence comes from the data obtained with NanoSIMS. The isotopic C maps do not show a C background (except for the film, which has been ignored in the images) in sections where acrylic has been removed. Instead, C is only observed in spots, that are systematically associated with the ^{15}N-enriched spots measured (see Fig. 7).

DISCUSSION

The three techniques we used to analyze the carbonaceous phases in two Stardust particles provide complementary information that is very helpful for understanding the nature of the phases that contain this C. From these analyses it was shown that the carbonaceous phases are definitely cometary. A terrestrial (contamination) origin is totally excluded because the carbonaceous phases are systematically associated with a pronounced enrichment in the isotope ^{15}N. The level of the $\delta^{15}N$ enrichment found in both Febo and Ada is comparable with values previously observed in some organic compounds in IDPs (Aléon et al. 2003; Floss et al. 2004, 2006) and meteorites (Busemann et al. 2006; Nakamura-Messenger et al. 2006) as well as in some other Stardust particles (McKeegan et al. 2006). The N and C isotopic compositions of the carbonaceous material of Ada and Febo are in the range observed for Tagish Lake organic globules (Fig. 15) and do not show any C isotopic anomalies. The O isotopic values measured in the minerals fayalite and crystalline SiO_2 of Ada and in the enstatite of Febo are in the range of meteoritic materials and are indistinguishable from other reported Stardust measurements (McKeegan et al. 2006), with the exception of the ^{16}O-rich refractory minerals found in the particle Inti (McKeegan et al. 2006; Zolensky et al. 2006), showing that these two particles do not contain presolar oxide or silicate grains.

The carbonaceous material in the particle Ada is also D-enriched and the δD value measured is in the range typically observed in meteoritic organic matter (Busemann et al. 2006; Nakamura-Messenger et al. 2006), in particular in organic molecules such as amino acids, alkanes and alkylbenzenes where D enrichment values were found to range from ~300‰ to ~4400‰ (Pizzarello and Huang 2005), suggesting that some of these organic molecules may be the carbonaceous carrier of the D anomaly found in Ada.

The δD value measured in Ada is also in the range typically observed in IDPs (Floss et al. 2006) and similar to the value previously reported in Stardust samples (McKeegan et al.

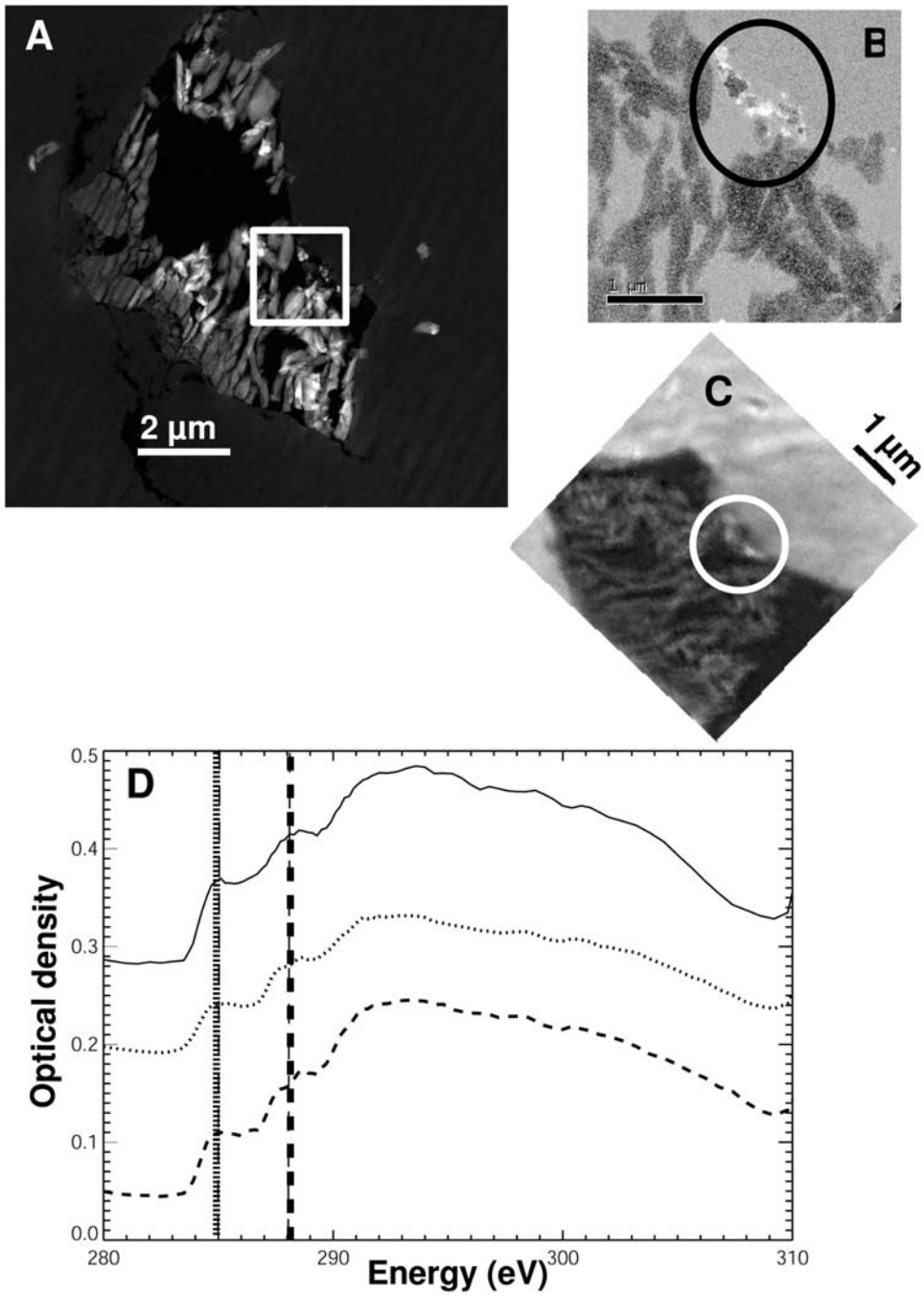

Fig. 12. Carbon XANES data of Ada. a) Micrograph of the whole particle obtained with HAADF detector. The square denotes the region where C-rich grains where found. b) EELS C map, showing inside the circle the C-rich area (brighter grains). c) C-XANES map, showing inside the circle the C-rich area (brighter grains). d) Plot with C-XANES spectra of three C-rich grains inside the circle in C).

2006). The size of the D-rich spot is also comparable to the size of D-rich hotspots found in some IDPs (Floss et al. 2006). However, unlike IDPs where H and N isotopic anomalies are not directly correlated (Floss et al. 2006), in the particle Ada the carbonaceous phase is also the host of both D and ^{15}N enrichments, suggesting that the host phase contains surviving molecular cloud material (Floss et al. 2006 and references therein).

The particle Febo, however, does not show any H isotopic anomaly. Organic matter in primitive meteorites and IDPs displays a wide range of H isotopic compositions, spanning from slightly lower than terrestrial values up to 50 times terrestrial. Moreover, there exist some IDPs that typically show ^{15}N-rich hotspots but do not show any D anomalies (Floss et al. 2006). Therefore, the isotopic variability observed between Febo and Ada reflects the wide

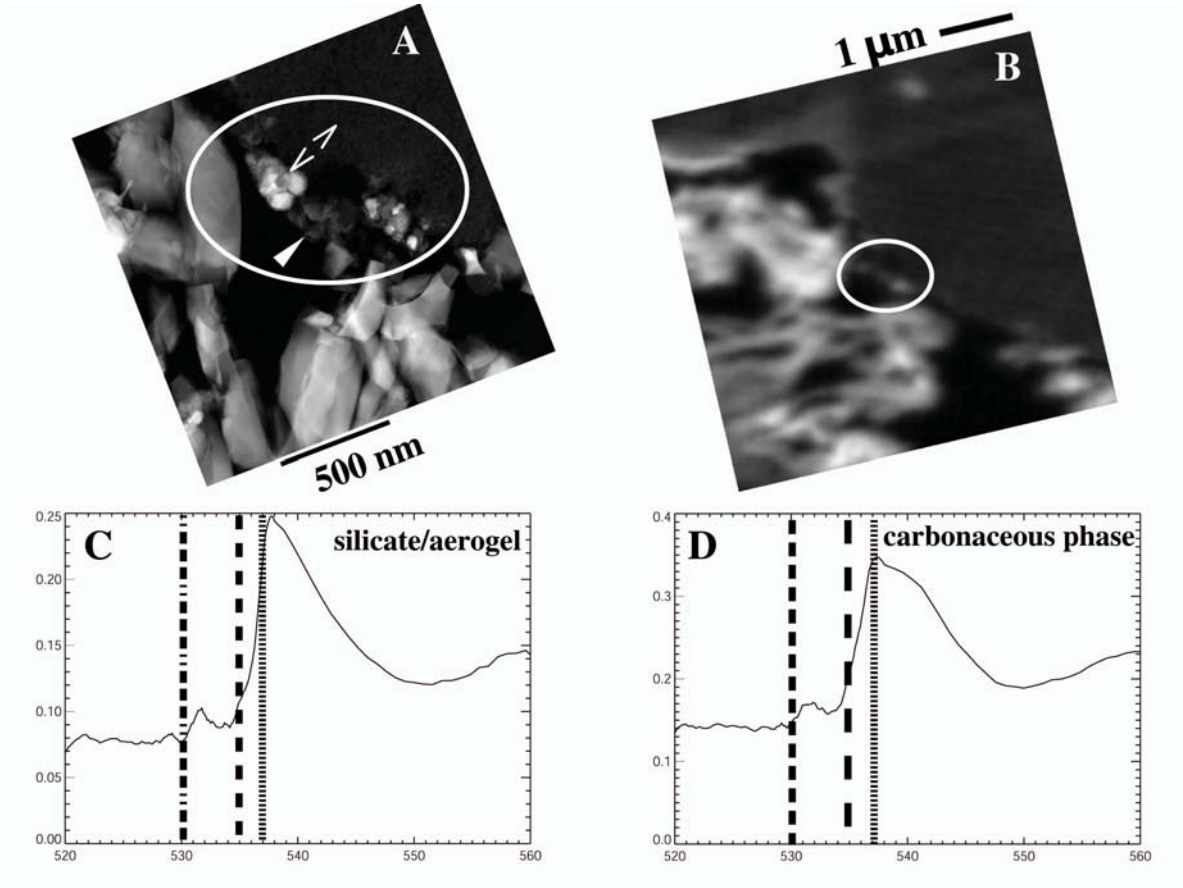

Fig. 13. Oxygen-XANES data of Ada. a) HAADF image. This image shows the high Z elements brighter, therefore, the silicates look brighter than the C-rich areas. The circle denotes the region where C-rich grains where found with EELS. It is clear from the difference in contrast in this image that besides C-rich grains in this region there are also silicate grains intermixed. The single arrow points to a C-rich grain (whose O-XANES is shown in (d) and the double arrow points from one arrow head to a silicate grain (or a piece of melted aerogel) and from the other arrow head to surrounding aerogel. b) O-XANES map, showing inside the circle the C-rich area (brighter grains). C) O-XANES spectrum of silicate/aerogel phase, showing a narrow peak centered at 537.8 eV. d) O-XANES spectrum of the carbonaceous phase, showing a broader peak centered at 537 eV.

variety of possible formation processes and subsequent alteration histories of organic matter in comets and meteorites.

Febo and Ada can be compared to the group of IDPs known as "isotopically normal" that was classified by Floss et al. (2006) based on their N isotopic compositions. This group of IDPs, like Ada and Febo, are characterized by having a normal bulk N isotopic composition with some ^{15}N-rich hotspots; they do not exhibit C isotopic anomalies and do not contain presolar silicate or oxide grains. However, the abundance of the carbonaceous phases found in both Febo and Ada is relatively low when compared with chondritic IDPs of similar size, given that the C is concentrated in small regions, no larger than 200 nm in size, and these regions are rare (no more than two to three grains are present in a single Wild 2 particle). Typically, the ^{15}N-rich carbonaceous phases in IDPs vary in size from 250–400 nm^2 (Floss et al. 2006).

Nevertheless, the sizes of the C-rich inclusions observed in Febo and Ada are comparable to the submicrometer-scale isotopically anomalous carbonaceous inclusions previously found in Tagish Lake (Nakamura-Messenger et al. 2006). In addition, the shape of the δ^{15}N-rich doughnut observed in Febo is also remarkably similar to the ^{15}N-rich, submicrometer, hollow organic globules recently reported in the Tagish Lake meteorite (Nakamura-Messenger et al. 2006). These materials all exhibit common isotopic signatures (δ^{15}N enrichments ≥200‰, D enrichments ≥500‰, and isotopically normal C) that point to low temperature (≤20 K) chemical fractionation, most likely to occur in a cold interstellar molecular cloud (Nakamura-Messenger et al. 2006).

The C in Ada is also concentrated in nanophases ≤200 nm in size which are found at the periphery of the particle (Fig. 2). Ada, composed of fayalite and tridymite, could be considered to be close to the mineralogy of some chondrules from type 3 ordinary chondrites that also contain an association of fayalite with silica (Wasson and Krot 1994). In this type of

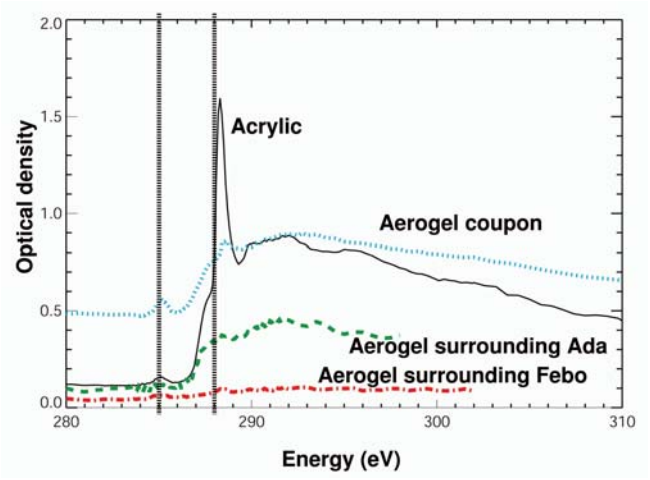

Fig. 14. Four C-XANES spectra are shown. The spectrum labeled "aerogel coupon" corresponds to a piece of bulk aerogel (courtesy of A. Butterworth). The spectrum labelled "acrylic" corresponds to a microtomed section of aerogel embedded in acrylic in which the acrylic has not been removed using chloroform. The spectrum labelled "aerogel surrounding Ada" corresponds to a section of the particle Ada surrounded by aerogel and embedded in acrylic, which was washed with chloroform and the acrylic dissolved. The spectrum labelled "aerogel surrounding Febo" corresponds to a section of the particle Febo surrounded by aerogel and embedded in acrylic, which was washed with chloroform and the acrylic dissolved. The spectrum labelled "acrylic" is dominated by a sharp, high peak at 288.5 eV that is absent in the other three spectra. Instead, the spectra of the aerogel have a small, broader peak at 288.5 eV. All four spectra have a small peak at 285 eV.

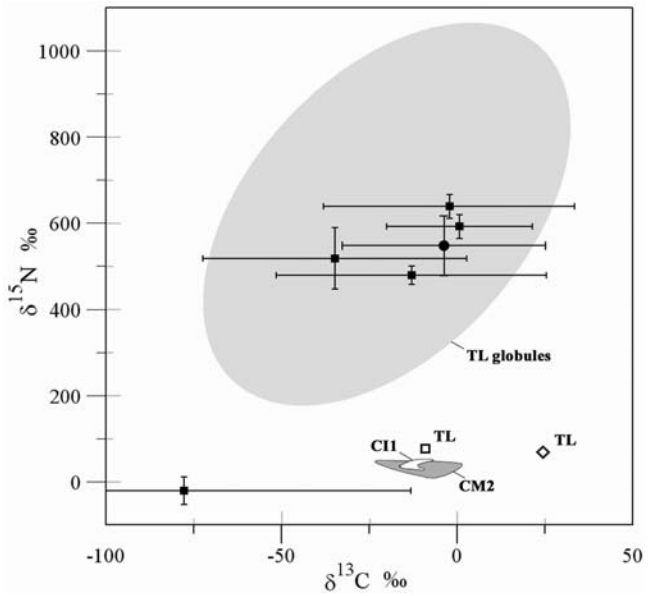

Fig. 15. Carbon and N isotopic compositions of Ada (filled circle) and Febo (filled squares) compared with ranges observed in the Tagish Lake (TL) organic globules (Nakamura-Messenger et al. 2006), TL whole rock (diamond), and organic matter (open square) (Grady et al. 2002), and CI1 and CM2 whole rocks (Kerridge 1985). The error bars are 1σ.

mineralogy, carbonaceous phases are unexpected. Perhaps the C we see was originally in a fine-grained C-rich matrix that was part of the particle before it impacted the aerogel. The matrix may have been vulnerable to the hypervelocity impact of the particle upon aerogel and may have been decomposed or highly altered, leaving behind the more robust phases of the original particle, the fayalite and tridymite crystals that we observe. The remnants of this matrix might be the C-rich nanophases that we found at the edge of these crystals.

The comparison of these two cometary particles with previous observations of some comets show some differences. For example, the $\delta^{15}N$ measured in Febo and Ada hotspots (from ~480‰ to ~640‰) is relatively smaller than the $\delta^{15}N$ of ~940‰ that was measured in the CN spectra of comets Hale-Bopp ($^{14}N/^{15}N = 140 \pm 35$) and LINEAR ($^{14}N/^{15}N = 140 \pm 30$) (Arpigny et al. 2003), suggesting that in Wild 2 the organic compounds are lighter than in Hale-Bopp and LINEAR. In addition, the abundance of C in Febo and Ada is significantly lower than expected considering that comets are generally thought to be relatively rich in C (Delsemme 1991; Mumma 1997; Huebner and Boice 1997; Gibb et al. 2007). However, there may at one time have been much more C present in other forms that was lost either by vaporization during impact or during the chloroform removal of the acrylic. Moreover, this work was done on terminal particles that are frequently made of solid rocks devoid of fine-grained matrix, which is more fragile. It is in the fine-grained material that the C is usually found in IDPs and meteorites. Studying particles with little or no fine-grained phases represents a strong bias in our study, because most of the fine-grained material of the comet may have been destroyed during collection. Febo is perhaps the first example of the fine-grained material of this comet, and so a straight comparison of Wild 2 particles with IDPs and meteorites is not yet possible. The rarity of carbonaceous phases in the terminal particles studied suggests that much of the C in comet Wild 2 may reside in volatile and/or labile carbonaceous compounds that were diluted in/or around the tracks in the aerogel. Indeed, aliphatic-rich organics were found along and around several tracks (Sandford et al. 2006) and Bajt et al. (unpublished data).

The carbonaceous material seems to be amorphous and may have been slightly heated, as seen by the subparallel fringes observed with HRTEM. However, the carbonaceous phases could not have been heated at temperatures ≥1000 °C given that the poorly ordered structure observed is very distinct from the order usually observed in severely heated C, such as graphite. This observation is further supported by the absence of a peak at 290 eV in the C-XANES spectra, typical of a graphitized C.

The C is present in a variety of compounds as seen in the diversity of C-XANES spectra from the different carbonaceous areas both between Febo and Ada and within a single particle. Some of these compounds are

likely to be organic, given that they contain N, as evidenced by the overlaps found in both the XANES and NanoSIMS N and C maps and the ^{15}N-enrichments associated with the C-rich phases. In addition, both Febo and Ada also present an overlap between C and O as it was observed from the C and O-XANES maps. The C-XANES spectrum of Ada and one of the Febo C-XANES spectra show a peak at 288.5 eV suggestive of a carbonyl (C=O) functional group, also consistent with the presence of organic material.

The C-XANES spectra of the two Stardust particles analyzed during this study show several differences when compared to C-XANES spectra from other solar system samples like meteorites and IDPs (Fig. 9). For example, the peak at 285 eV in both Febo and Ada is broader and lower than the peak at 285 eV in all other samples compared. Both IDPs have a peak at 286.5 eV and a peak at 290 eV that are absent in Febo and Ada. The relative heights of the peaks at 285 eV and 288.5 eV are different in Febo and Ada from Murchison, Orgueil, and Tagish Lake. These differences may indicate that the organic compounds found in Febo and Ada are a new type of organic material. Alternatively, these distinctiveness may indicate that the organics in Febo and Ada were heated and severely altered during hypervelocity impact into the aerogel or that they were altered by the chloroform, and this would be a reason why they look different from the known organics of IDPs and meteorites.

The carbonaceous compounds found during the present study also look different from the ones found by C-XANES in six different Wild 2 particles and reported by Sandford et al. (2006). The comparison of the C-XANES spectra of both Febo and Ada to C-XANES spectra obtained in other Wild 2 particles during the PET period is difficult given that none of the spectra are similar. One reason for such a discrepancy is that the carbonaceous material studied in the present work is a solid phase closely associated with minerals identified as cometary and that is found in a terminal particle, whereas the results reported in Sandford et al. (2006) discuss a volatile organic phase present in grains that were extracted from along the track but that are not necessarily the TP. Another reason to explain these differences could be the sample preparation process, which could be altering and/or dissolving some of the compounds responsible for those features in the spectra of the six Wild 2 particles reported in Sandford et al. (2006) that are absent in the Febo and Ada spectra. But most probably, our results do not seem similar to the ones reported by Sandford et al. (2006) simply due to the intrinsic variability of the Wild 2 samples. We discussed this variability in the Carbon, Nitrogen, and Oxygen X-Ray Imaging and XANES Analysis section, and showed that variability is observed between both Febo and Ada and even within a few nm in the particle Febo.

CONCLUSIONS

A coordinated study involving three analytical techniques (TEM, NanoSIMS, and XANES) of two Stardust particles, Febo and Ada, has established the presence of C in both particles. We found that the carbonaceous phases remaining after exposure to chloroform consist of small ~100–200 nm grains that are rare, because only two to three grains are present in a single particle. The C is amorphous and presents subparallel fringes suggesting that it was slightly heated.

The carbonaceous phases are systematically associated with ^{15}N enrichments, consistent with an organic, cometary material. In the particle Ada the carbonaceous phase is also associated with a D enrichment whose value is comparable to enrichments observed in IDPs. The C-rich areas are sometimes associated with O and show the presence of a carbonyl (C=O) feature at 288.5 eV, which also supports their organic nature. Although the size and level of the ^{15}N enrichment found in these C-rich areas is comparable with C-rich inclusions previously reported in IDPs, the C-XANES spectra of the organic materials in Febo and Ada is different from the ones observed in IDPs and carbonaceous chondrites.

Given that the carbonaceous phases are rare (as seen with the TEM) and very small, we plan to continue an extensive and coordinated search for C in several more Stardust particles to better assess its nature and abundance in the comet Wild 2.

Acknowledgments—This work was funded by NASA grants NNM05AA19G and NNX07AM78G. We thank the Stardust PET and the JSC curation facility for providing the samples. We are grateful to H. Busemann, F. Stadermann, and an anonymous reviewer for their comments which helped so much to improve this manuscript.

REFERENCES

Aléon J., Robert F., Chaussidon M., and Marty B. 2003. Nitrogen isotopic composition of macromolecular organic matter in interplanetary dust particles. *Geochimica et Cosmochimica Acta* 67:3773–3783.

Arpigny C., Jehin E., Manfroid J., Hutsemékers D., Schulz R., Stüwe J. A., Zucconi J.-M., and Ilyin I. 2003. Anomalous nitrogen isotope ratio in comets. *Science* 301:1522–1525.

Brownlee D. E., Tsou P., Anderson J. D., Hanner M. S., Newburn R. L., Sekanina Z., Clark B. C., Hörz F., Zolensky M. E., Kissel J., McDonnell J. A. M., Sandford S. A., and Tuzzolino A. J. 2003. Stardust: Comet and interstellar dust sample return mission. *Journal of Geophysical Research* 108:1–15.

Brownlee D., Tsou P., Aléon J., Alexander C. M. O'D., Araki T., Bajt S., Baratta G. A., Bastien R., Bland P., Bleuet P., Borg J., Bradley J. P., Brearley A., Brenker F., Brennan S., Bridges J. C., Browning N. D., Brucato J. R., Bullock E., Burchell M. J., Busemann H., Butterworth A., Chaussidon M., Cheuvront A., Chi M., Cintala M. J., Clark B. C., Clemett S. J., Cody G., Colangeli L., Cooper G., Cordier P., Daghlian C., Dai Z., D'Hendecourt L., Djouadi Z., Dominguez G., Duxbury T.,

Dworkin J. P., Ebel D. S., Economou T. E., Fakra S., Fairey S. A. J., Fallon S., Ferrini G., Ferroir T., Fleckenstein H., Floss C., Flynn G., Franchi I. A., Fries M., Gainsforth Z., Gallien J.-P., Genge M., Gilles M. K., Gillet Ph., Gilmour J., Glavin D. P., Gounelle M., Grady M. M., Graham G. A., Grant P. G., Green S. F., Grossemy F., Grossman L., Grossman J. N., Guan Y., Hagiya K., Harvey R., Heck P., Herzog G. F., Hoppe P., Hörz F., Huth J., Hutcheon I. D., Ignatyev K., Ishii H., Ito M., Jacob D., Jacobsen C., Jacobsen S., Jones S., Joswiak D., Jurewicz A., Kearsley A. T., Keller L. P., Khodja H., Kilcoyne A. L. D., Kissel J., Krot A., Langenhorst F., Lanzirotti A., Le L., Leshin L. A., Leitner J., Lemelle L., Leroux H., Liu M.-C., Luening K., Lyon I., MacPherson G., Marcus M. A., Marhas K., Marty B., Matrajt G., McKeegan K., Meibom A., Mennella V., Messenger K., Messenger S., Mikouchi T., Mostefaoui S., Nakamura T., Nakano T., Newville M., Nittler L. R., Ohnishi I., Ohsumi K., Okudaira K., Papanastassiou D. A., Palma R., Palumbo M. E., Pepin R. O., Perkins D., Perronnet M., Pianetta P., Rao W., Rietmeijer F. J. M., Robert F., Rost D., Rotundi A., Ryan R., Sandford S. A., Schwandt C. S., See T. H., Schlutter D., Sheffield-Parker J., Simionovici A., Simon S., Sitnitsky I., Snead C. J., Spencer M. K., Stadermann F. J., Steele A., Stephan T., Stroud R., Susini J., Sutton S. R., Suzuki Y., Taheri M., Taylor S., Teslich N., Tomeoka K., Tomioka N., Toppani A., Trigo-Rodríguez J. M., Troadec D., Tsuchiyama A., Tuzzolino A. J., Tyliszczak T., Uesugi K., Velbel M., Vellenga J., Vicenzi E., Vincze L., Warren J., Weber I., Weisberg M., Westphal A. J., Wirick S., Wooden D., Wopenka B., Wozniakiewicz P., Wright I., Yabuta H., Yano H., Young E. D., Zare R. N., Zega T., Ziegler K., Zimmerman L., Zinner E., and Zolensky M. 2006. Comet 81P/Wild 2 under a microscope. *Science* 314:1711–1716.

Buseck R. P. and Bo-Jun H. 1985. Conversion of carbonaceous material to graphite during metamorphism. *Geochimica et Cosmochimica Acta* 49:2003–2016.

Buseck R. P., Bo-Jun H., and Keller L. P. 1987. Electron microscope investigations of the structure of annealed carbons. *Journal Energy Fuels* 1:105–110.

Busemann H., Young A. F., Alexander C. M. O'D., Hoppe P., Mukhopadhyay S., and Nittler L. R. 2006. Interstellar chemistry recorded in organic matter from primitive meteorites. *Science* 312:727–730.

Delsemme A. H. 1991. Nature and history of the organic compounds in comets—An astrophysical view. In *Comets in the post-Halley era*, edited by Newburn R. L. Jr., Neugebauer M., and Rahe J. pp. 377–428.

Floss C., Stadermann F., Bradley J., Dai Z., Bajt S., and Graham G. 2004. Carbon and nitrogen isotopic anomalies in an anhydrous interplanetary dust particle. *Science* 303:1355–1358.

Floss C., Stadermann F. J., Bradley J. P., Dai Z. R., Bajt S., Graham G., and Lea A. S. 2006. Identification of isotopically primitive interplanetary dust particles: A NanoSIMS isotopic imaging study. *Geochimica et Cosmochimica Acta* 70:2371–2399.

Flynn G. J., Bleuet P., Borg J., Bradley J. P., Brenker F. E., Brennan S., Bridges J., Brownlee D. E., Bullock E. S., Burghammer M., Clark B. C., Dai Z. R., Daghlian C. P., Djouadi Z., Fakra S., Ferroir T., Floss C., Franchi I. A., Gainsforth Z., Gallien J.-P., Gillet P., Grant P. G., Graham G. A., Green S. F., Grossemy F., Heck P. R., Herzog G. F., Hoppe P., Hörz F., Huth J., Ignatyev K., Ishii H. A., Janssens K., Joswiak D., Kearsley A. T., Khodja H., Lanzirotti A., Leitner J., Lemelle L., Leroux H., Luening K., MacPherson G. J., Marhas K. K., Marcus M. A., Matrajt G., Nakamura T., Nakamura-Messenger K., Nakano T., Newville M., Papanastassiou D. A., Pianetta P., Rao W., Riekel C., Rietmeijer F. J. M., Rost D., Schwandt C. S., See T. H., Sheffield-Parker J., Simionovici A., Sitnitsky I., Snead C. J., Stadermann F. J., Stephan T., Stroud R. M., Susini J., Suzuki Y., Sutton S. R., Taylor S., Teslich N., Troadec D., Tsou P., Tsuchiyama A., Uesugi K., Vekemans B., Vicenzi E. P., Vincze L., Westphal A. J., Wozniakiewicz P., Zinner E., and Zolensky M. E. 2006. Elemental Compositions of comet 81P/Wild 2 samples collected by Stardust. *Science* 314:1731–1735.

Flynn G. J., Keller L. P., Feser M., Wirick S., and Jacobsen C. 2003. The origin of organic matter in the solar system: Evidence from the interplanetary dust particles. *Geochimica et Cosmochimica Acta* 67:4791–4806.

Flynn G. J., Keller L., Jacobsen C., and Wirick S. 2004. An assessment of the amount and types of organic matter contributed to the Earth by interplanetary dust. *Advances in Space Research* 33:57–66.

Gibb E. L., Disanti M. A., Magee-Sauer K., Dello Russo N., Bonev B. P., and Mumma M. J. 2007. The organic composition of C/2001 A2 (LINEAR). *Icarus* 188:224–232.

Grady M. M., Verchovsky A. B., Franchi I. A., Wright I. P., and Pillinger C. T. 2002. Light element geochemistry of the Tagish Lake CI2 chondrite: Comparison with CI1 and CM2 meteorites. *Meteoritics & Planetary Science* 37:713–735.

Hörz F., Bastien R., Borg J., Bradley J. P., Bridges J. C., Brownlee D. E., Burchell M. J., Chi M., Cintala M. J., Dai Z. R., Djouadi Z., Dominguez G., Economou T. E., Fairey S. A. J., Floss C., Franchi I. A., Graham G. A., Green S. F., Heck P., Hoppe P., Huth J., Ishii H., Kearsley A. T., Kissel J., Leitner J., Leroux H., Marhas K., Messenger K., Schwandt C. S., See T. H., Snead C., Stadermann F. J., Stephan T., Stroud R., Teslich N., Trigo-Rodríguez J. M., Tuzzolino A. J., Troadec D., Tsou P., Warren J., Westphal A., Wozniakiewicz P., Wright I., and Zinner E. 2006. Impact features on Stardust: Implications for comet 81P/Wild 2 dust. *Science* 314:1716–1719.

Huebner W. and Boice D. 1997. Polymers and other macromolecules in comets. In *Comets and the origin and evolution of life*. New York: Springer. pp. 111–129.

Jacobsen G., Flynn G., Wirick S., and Zimba C. 2000. Soft X-ray spectroscopy from image sequences with sub-100 nm spatial resolution. *Journal of Microscopy* 197:173–184.

Keller L. P., Bajt S., Baratta G. A., Borg J., Bradley J. P., Brownlee D. E., Busemann H., Brucato J. R., Burchell M., Colangeli L., D'Hendecourt L., Djouadi Z., Ferrini G., Flynn G., Franchi I. A., Fries M., Grady M. M., Graham G. A., Grossemy F., Kearsley A., Matrajt G., Nakamura-Messenger K., Mennella V., Nittler L., Palumbo M. E., Stadermann F. J., Tsou P., Rotundi A., Sandford S. A., Snead C., Steele A., Wooden D., and Zolensky M. 2006. Infrared spectroscopy of comet 81P/Wild 2 samples returned by Stardust. *Science* 314:1728–1731.

Keller L. P., Messenger S., Flynn G. J., Clemett S., Wirick S., and Jacobsen C. 2004. The nature of molecular cloud material in interplanetary dust. *Geochimica et Cosmochimica Acta* 68:2577–2589.

Kerridge J. F. 1985. Carbon, hydrogen and nitrogen in carbonaceous chondrites. Abundances and isotopic compositions in bulk samples. *Geochimica et Cosmochimica Acta* 49:1707–1714.

Lerotic M., Jacobsen C., Schä fer T., and Vogt S. 2004. Cluster analysis of soft X-ray spectromicroscopy data. *Ultramicroscopy* 100:35–57.

Matrajt G., Brownlee D. E., Joswiak D. J., and Taylor S. 2005. Atmospheric entry heating effects on organic carbonaceous phases of IDPs and polar micrometeorites: An EELS study (abstract #1553). 36th Lunar and Planetary Science Conference. CD–ROM.

Matrajt G., Flynn G. J., Bradley J., and Maurette M. 2001. FTIR and

STXM detection of organic carbon in scoriaceous-type Antarctic micrometeorites (abstract #1336). 32nd Lunar and Planetary Science Conference. CD–ROM.

Matrajt G. and Brownlee D. 2006. Acrylic embedding of Stardust particles encased in aerogel. *Meteoritics & Planetary Science* 41: 1715–1720.

McKeegan K. D., Aléon, J., Bradley J., Brownlee D., Busemann H., Butterworth A., Chaussidon M., Fallon S., Floss C., Gilmour J., Gounelle M., Graham G., Guan Y., Heck P. R., Hoppe P., Hutcheon I. D., Huth J., Ishii H., Ito M., Jacobsen S. B., Kearsley A., Leshin L. A., Liu M.-C., Lyon I., Marhas K., Marty B., Matrajt G., Meibom A., Messenger S., Mostefaoui S., Mukhopadhyay S., Nakamura-Messenger K., Nittler L., Palma R., Pepin R. O., Papanastassiou D. A., Robert F., Schlutter D., Snead C. J., Stadermann F. J., Stroud R., Tsou P., Westphal A., Young E. D., Ziegler K., Zimmermann L., and Zinner E. 2006. Isotopic compositions of cometary matter returned by Stardust. *Science* 314:1724–1728.

Messenger S., Keller L., Nakamura-Messenger K., and Ito M. 2007. The abundance and distribution of presolar materials in cluster IDPs (abstract #2122). 38th Lunar and Planetary Science Conference. CD–ROM.

Mumma M. 1997. Organics in comets. In *Astronomical and biochemical origins and the search for life in the universe*. Bologna: Editrice Compositori. pp. 121–142.

Nakamura-Messenger K., Messenger S., Keller L., Clemett S., and Zolensky M. 2006. Organic globules in the Tagish Lake meteorite: Remnants of the protosolar disk. *Science* 314:1439–1442.

Pizzarello S. and Huang Y. 2005. The deuterium enrichment of individual amino acids in carbonaceous meteorites: A case for the presolar distribution of biomolecule precursors. *Geochimica et Cosmochimica Acta* 69:599–605.

Sandford S. A., Alé on J., Alexander C. M. O. D., Araki T., Bajt S., Baratta G. A., Borg J., Bradley J. P., Brownlee D. E., Brucato J. R., Burchell M. J., Busemann H., Butterworth A., Clemett S. J., Cody G., Colangeli L., Cooper G., D'Hendecourt L., Djouadi Z., Dworkin J. P., Ferrini G., Fleckenstein H., Flynn G. J., Franchi I. A., Fries M., Gilles M. K., Glavin D. P., Gounelle M., Grossemy F., Jacobsen C., Keller L. P., Kilcoyne A. L. D., Leitner J., Matrajt G., Meibom A., Mennella V., Mostefaoui S., Nittler L. R., Palumbo M. E., Papanastassiou D. A., Robert F., Rotundi A., Snead C. J., Spencer M. K., Stadermann F. J., Steele A., Stephan T., Tsou P., Tyliszczak T., Westphal A. J., Wirick S., Wopenka B., Yabuta H., Zare R. N., and Zolensky M. E. 2006. Organics captured from comet 81P/Wild 2 by the Stardust spacecraft. *Science* 314:1720–1724.

Wasson J. T. and Krot A. N. 1994. Fayalite-silica association in unequilibrated ordinary chondrites: Evidence for aqueous alteration on a parent body. *Earth and Planetary Science Letters* 122:403–416.

Westphal A. J., Snead C., Butterworth A., Graham G. A., Bradley J. P., Bajt S., Grant P. G., Bench G., Brennan S., and Pianetta P. 2004. Aerogel keystones: Extraction of complete hypervelocity impact events from aerogel collectors. *Meteoritics & Planetary Science* 39:1375–1386.

Zolensky M. E., Zega T. J., Yano H., Wirick S., Westphal A. J., Weisberg M. K., Weber I., Warren J. L., Velbel M. A., Tsuchiyama A., Tsou P., Toppani A., Tomioka N., Tomeoka K., Teslich N., Taheri M., Susini J., Stroud R., Stephan T., Stadermann F. J., Snead C. J., Simon S. B., Simionovici A., See T. H., Robert F., Rietmeijer F. J. M., Rao W., Perronnet M. C., Papanastassiou D. A., Okudaira K., Ohsumi K., Ohnishi I., Nakamura-Messenger K., Nakamura T., Mostefaoui S., Mikouchi T., Meibom A., Matrajt G., Marcus M. A., Leroux H., Lemelle L., Le, L., Lanzirotti A., Langenhorst F., Krot A. N., Keller L. P., Kearsley A. T., Joswiak D., Jacob D., Ishii H., Harvey R., Hagiya K., Grossman L., Grossman J. N., Graham G. A., Gounelle M., Gillet P., Genge M. J., Flynn G., Ferroir T., Fallon S., Ebel D. S., Dai Z. R., Cordier P., Clark B., Chi M., Butterworth A. L., Brownlee D. E., Bridges J. C., Brennan S., Brearley A., Bradley J. P., Bleuet P., Bland P. A., and Bastien R. 2006. Mineralogy and petrology of comet 81P/Wild 2 nucleus samples. *Science* 314:1735–1739.